Am J Transl Res 2020;12(12):8225-8246
www.ajtr.org /ISSN:1943-8141/AJTR0115227

Original Article

Long non-coding RNA AFAP1-AS1 promotes cell growth and inhibits apoptosis by binding to specific proteins in germinal center B-cell-like diffuse large B-cell lymphoma

Hongyu Gao[1], Ying Sun[1], Jiawen Chen[1], Hong Jin[2], Wei Yang[1]

[1]*Department of Hematology, Shengjing Hospital Affiliated to China Medical University, Shenyang 110000, Liaoning, P. R. China;* [2]*Department of Pathogen Biology, China Medical University, Shenyang 110000, Liaoning, P. R. China*

Received May 28, 2020; Accepted December 2, 2020; Epub December 15, 2020; Published December 30, 2020

Abstract: Germinal center B-cell-like diffuse large B-cell lymphoma (GCB-DLBCL) is a common subtype of lymphoma in adults. Previously, we found that actin filament-associated protein 1-antisense RNA 1 (AFAP1-AS1) is among the most overexpressed lncRNAs in GCB-DLBCL. In this study, we explored its biological functions and molecular mechanisms in the progression of GCB-DLBCL. We discovered, via bioinformatics, that patients with a high expression of AFAP1-AS1 had significantly poor disease-free survival (DFS) and overall survival (OS). Subsequent assays demonstrated that AFAP1-AS1 knockdown inhibited cell proliferation and prompted arrest of the G0/G1 cell cycle and apoptosis in GCB-DLBCL cell lines. Proteomics analysis indicated that hundreds of proteins were deregulated after AFAP1-AS1 knockdown and KEGG pathway analysis revealed that the deregulated proteins belonged to multiple signaling pathways, such as "B-cell receptor signaling pathway". Moreover, in the comprehensive identification of proteins that bind to RNA (by ChIRP-MS), several proteins associated with RNA splicing were identified (e.g., SFPQ, NONO, SRSF2, SRSF6, and KHSRP) that could specifically bind to AFAP1-AS1, which was confirmed by parallel reaction monitoring assay (PRM). Conclusively, we demonstrated that AFAP1-AS1 is a possible prognostic marker of poor outcomes in GCB-DLBCL patients and could modulate gene expression through connecting to specific proteins to practice its oncogenic role in GCB-DLBCL.

Keywords: AFAP1-AS1, germinal center B-cell-like diffuse large B-cell lymphoma, apoptosis, alternative splicing

Introduction

Diffuse large B-cell lymphoma (DLBCL), the most common type of non-Hodgkin lymphoma (NHL) in adults, accounts for 35 to 40% of all NHL [1]. It is a heterogeneous lymphoma, consisting of several subtypes with quite different molecular signatures [1]. The "germinal center B-cell (GCB)-like" subtype is linked to chromosomal translocations, like t(14;18)(q32;q21) [2], and mutations in histone-modifying genes, including enhancer of zeste homolog 2 (EZH2) [3] and CREB binding protein (CREBBP) [4]. Over 50% of the patients with GCB-DLBCL can be cured with the routine rituximab-based regimen; however, a consistent portion of patients eventually relapse. Therefore, increased knowledge of the mechanisms related to the development of GCB-DLBCL is needed.

Accumulating data suggest that long non-coding RNAs (lncRNAs) can act as tumor suppressors or oncogenes in human malignancies [5-7]. In our previous research, we studied the lncRNA expression profiles in GCB-DLBCL cells by microarray. We found that actin filament-associated protein 1-antisense RNA 1 (AFAP1-AS1) was one of the most overexpressed lncRNAs [8]. AFAP1-AS1 is 6,810 bp in length and maps to the 4p16.1 region of chromosome 4, which is transcribed from the AFAP1 gene locus' antisense strand and regulates AFAP1 expression [9]. AFAP1-AS1 is upregulated and related to adverse clinical prognosis in various cancers [9-13]. Furthermore, the knockdown of AFAP1-AS1 suppresses proliferation in cells, invasion, migration, and facilitates apoptosis and cell cycle arrest [10, 11, 14-17]. However, there is limited knowledge of the involvement of AFAP1-AS1 in the occurrence and progression of GCB-DLBCL.

In the present study, we verified the expression levels of AFAP1-AS1 in a large clinical sample

and investigated its prognostic value by data mining in the TCGA database. Subsequently, we explored the biological functions of AFAP1-AS1 related to progression of the cell cycle, apoptosis, and cell proliferation in GCB-DLBCL cells. We also identified the amount of expression of several apoptosis and cell cycle-related proteins after AFAP1-AS1 downregulation. Finally, we performed label-free quantitative proteomics and comprehensive detection of RNA-binding proteins with mass spectrometry (ChIRP-MS) to identify the signaling pathways and binding proteins for AFAP1-AS1 in GCB-DLBCL.

Materials and methods

Cell culture

GCB-DLBCL cell lines (OCI-ly1 and OCI-ly19) derived from humans, were purchased from the Cell Resource Center of the Shanghai Institutes for Biological Sciences. Following, culture of the cells in Dulbecco's Modified Eagle Medium (DMEM)-high glucose supplemented by 10% fetal bovine serum (FBS, Gibco, CA, USA), they were incubated at 37°C in a dampened incubator with CO_2 of 5%.

Quantitative reverse transcription-polymerase chain reaction (qRT-PCR)

Trizol reagent (Invitrogen, CA, USA) was used to extract the total RNA. The extracted RNA was quantified by a NanoDrop ND-1000 spectrophotometer and the fraction of uptake at 260 and 280 nm determined the purity. To prepare the cDNA, SuperScript™ III reverse transcriptase (Invitrogen, CA, USA) was used in accordance with the manufacturer's instructions. The SYBR-Green Kit (Invitrogen, CA, USA) and Rotor-Gene 3000 Real-time PCR Detection System (Corbett Research, Brisbane, Australia) were used to perform quantitative RT-PCR in accordance with the manufacturer's protocol.

AFAP1-AS1 knockdown by shRNA adenovirus transduction

Three short hairpin RNAs (shRNAs) targeting AFAP1-AS1 and control shRNA were designed and constructed by Hanbio Biotechnology. The shRNA sequences are presented in Supplementary Table 1. OCI-ly1 and OCI-ly19 cells were transduced with adenovirus containing sh-AFAP1-AS1#1, sh-AFAP1-AS1#2, sh-AFAP1-AS1#3, or sh-NC in DMEM, containing 5% FBS and 7 μg/mL polybrene, at a multiplicity of infection (MOI) of 200 plaque-forming units per cell. At 48 h after transduction, the cells were retrieved. The transduction efficiency was observed by fluorescence microscopy and the effectiveness of interference of the sh-AFAP1-AS was confirmed through qRT-PCR.

Cell proliferation assay

The proliferation of cells was analyzed with the Cell Counting Kit-8 Kit (CCK-8, Dojin, Kumamoto, Japan). Forty-eight hours after transduction, the cells were transferred to 96-well plates with 90 μL culture medium at the density of 2,000 cells per well and there were three duplicates for every sample. Every well was supplemented with 10 μL CCK-8 solution at pre-determined time slots. Then, the plates were incubated for the duration of 2 h at 37°C, followed by the measurement of the absorbance at 450 nm with a SpectraMax M5 Microplate Reader.

Apoptosis assay

Analysis of apoptosis was performed with the Annexin V-PE/7AAD Kit (Southern Biotech, Birmingham, AL). Forty-eight hours after transduction, cells were washed twice with 4°C PBS. Thereafter, the cells were retrieved and stained by using Annexin V-PE/7AAD in accordance with the manufacturer's protocol. Apoptosis was analyzed with flow cytometry by Flowjo 7.6 software (BD Biosciences, CA, USA).

Cell cycle analysis

The Cell Cycle and Apoptosis Analysis Kit (Beyotime, Shanghai, China) were used to evaluate the cell cycle. After 48 h of transduction and then washing the cells twice with 4°C PBS, they were collected and fixated in 75% ethanol at 4°C for 24 h. After washing, the cells together with RNase A were incubated for 30 min at 37°C. Subsequently, propidium iodide was used to stain the cells in the dark at room temperature for 30 min. The cell cycle was evaluated with flow cytometry using Flowjo 7.6 software.

Label-free quantitative proteomics

After digestion with trypsin, each sample was separated by high-performance liquid chromatography (HPLC) with a nanoliter flow rate. The chromatographic column was equilibrated with 95% liquid A. First, the sample was loaded into the pre-column of the mass spectrometer by

an automatic sampler and then separated by the analytical column. Each sample was separated by capillary HPLC and then the Q-Exactive HF mass spectrometer (Thermo Scientific) was used to analyze them.

Comprehensive detection of RNA-binding proteins with mass spectrometry (ChIRP-MS)

ChIRP-MS is the best approach to discover target proteins that directly bind to RNA. Protein-RNA interactions were detected as per manufacturer's instructions. The enriched proteins were analyzed with liquid chromatography-tandem mass spectrometry (LC-MS/MS). Additional information is provided in the Supplementary Materials.

Bioinformatics analysis

Processing of the data in The Cancer Genome Atlas (TCGA) database: The Cancer Genome Atlas (TCGA) database was accessed to retrieve data on RNA sequencing and clinical information for DLBCL. The samples were separated into low- and high-expression groups, with the median AFAP1-AS1 expression value set as the threshold value. The overall survival (OS) and disease-free survival (DFS) analysis was conducted with the Kaplan-Meier curve and log-rank test using the R package "survival".

Gene Ontology (GO), Kyoto Encyclopedia of Genes and Genomes (KEGG), and Eukaryotic Orthologous Groups (KOG) function classification analysis: To search for shared functions among genes, Gene Ontology (GO) (http://www.geneontology.org/), Kyoto Encyclopedia of Genes and Genomes (KEGG) (http://www.kegg.jp/kegg/pathway.html), and Eukaryotic Orthologous Groups (KOG) function classification (ftp://ftp.ncbi.nih.gov/pub/COG/KOG) analysis were performed to identify predominant biological themes.

Protein-protein interaction analysis: STRING refers to a database of protein-protein interactions, which includes functional and physical associations. These are based on computational prediction, transfer of knowledge among organisms, and interactions obtained from additional databases.

Western blotting

The total proteins from cells were derived on ice with RIPA buffer containing protease and phosphatase inhibitors (Beyotime Institute of Biotechnology, Shanghai, China). The extracts underwent sodium dodecyl sulfate-polyacrylamide gel electrophoresis (SDS-PAGE), followed by transfer onto PVDF membranes. Then the membranes were incubated overnight at 4°C with primary antibodies. The primary antibodies for cyclin D1, cyclin E1, cleaved-caspase3, Bcl-2, Bax, BTK, p-BTK, and DRP1 were obtained from Cell Signaling Technology (CST). GAPDH or β-actin antibody served as loading control. Immunoblots were performed with an ECL detection reagent.

Parallel reaction monitoring (PRM)

The separation of peptides was achieved with the nano-UPLC liquid phase system, EASY-nLC1200, and identified with an online mass spectrometer (Q-Exactive). The duration of the analysis was 120 min/sample in the positive ion detection mode. For the acquisition method of PRM, the resolution of MS2 at m/z@200 was 17,500, the AGC was 5E+4, and the maximum ion implantation time (Max IT) was 200 ms. The collected PRM data was transferred to Skyline for extraction of transition.

Statistical analysis

Experimental data have been presented as the mean ± standard deviation (SD). Comparisons among two different groups were analyzed using the Chi-square test or Student's t-test. *P*-value < 0.05 was regarded as statistically significant. SPSS 20.0 software was used to perform statistical analysis.

Results

AFAP1-AS1 was upregulated in GCB-DLBCL and related to poor prognosis

In our previous work, we demonstrated that AFAP1-AS1 was upregulated in the GCB-DLBCL cell lines (OCI-ly1 and OCI-ly19) and tissues compared to the controls using microarray and qRT-PCR [8]. In the current study, we verified the expression levels of AFAP1-AS1 in a larger cohort and investigated its clinical values by data mining the TCGA database. Our results indicate that, in DLBCL tissues, AFAP1-AS1 was upregulated significantly compared to control tissue ($\log_2$ fold change = 4.041, $P < 0.05$), which was consistent with our previous results (**Figure 1A**).

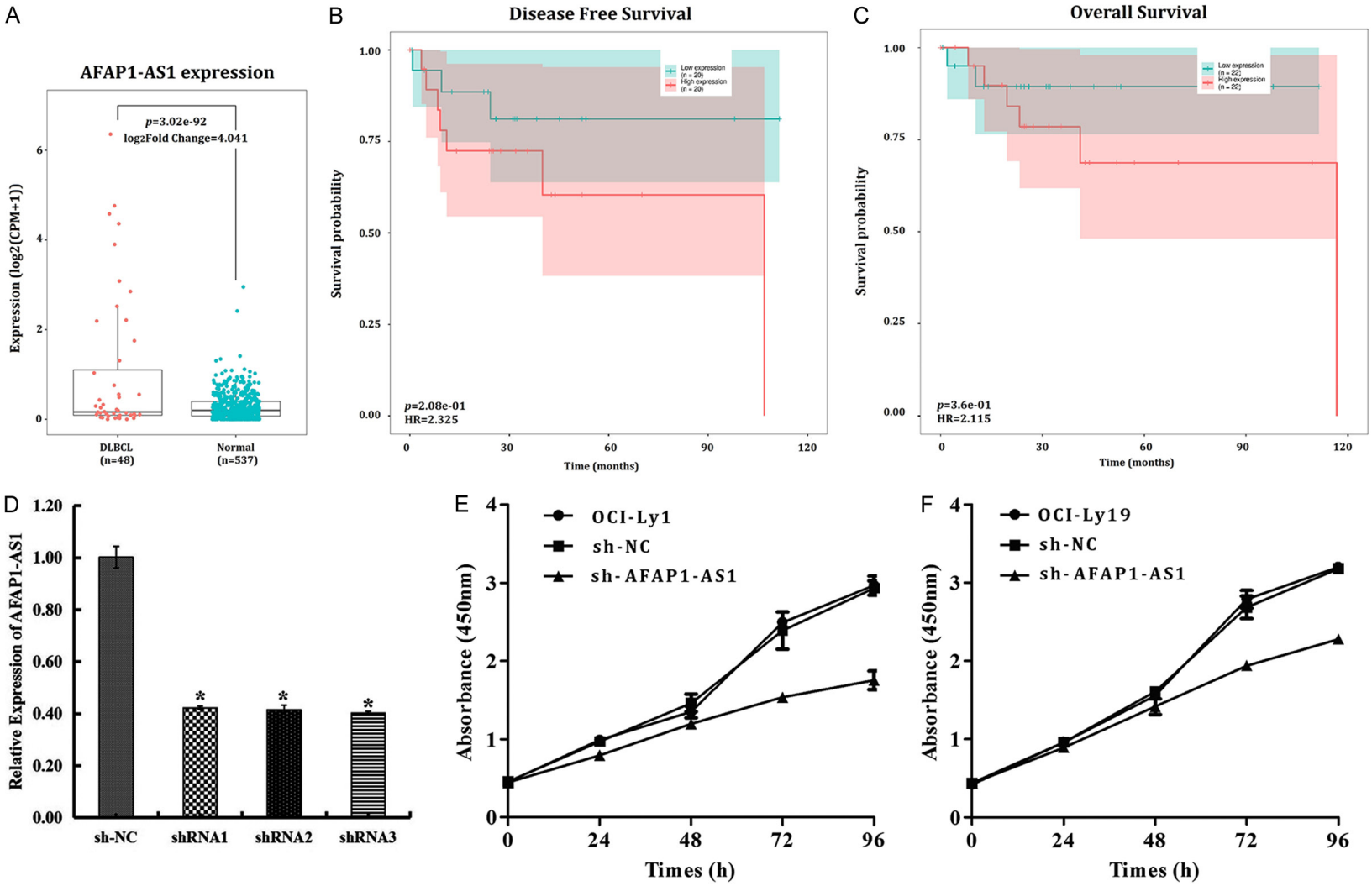

Figure 1. High expression of AFAP1-AS1 in GCB-DLBCL was related to poor prognosis and high cell proliferation. According to the data from the TCGA database, there was overexpression of AFAP1-AS1 in DLBCL tissues (A). The Kaplan-Meier analysis demonstrated that a high AFAP1-AS1 expression was related to poor disease-free survival (B) and poor overall survival (C) of DLBCL patients. The expression levels of AFAP1-AS1 in OCI-ly1 cells were detected by qRT-PCR following sh-NC, sh-AFAP1-AS1#1, sh-AFAP1-AS1#2, or sh-AFAP1-AS1#3 adenovirus transduction (D). Proliferation of the cells was determined by the CCK-8 assay in OCI-ly1 (E) and OCI-ly19 cells (F) following sh-NC or sh-AFAP1-AS1 adenovirus transduction.

Table 1. Clinical characters between the high-expression group and the low-expression group

Characteristics	High expression (n = 24)	Low expression (n = 24)	χ^2	*P* value
Age			2.0979021	0.1475014
< 60 y	16	10		
≥ 60 y	8	14		
Gender			0.08391608	0.77205897
Female	14	12		
Male	10	12		
Race			1.25670498	0.53346997
Asian	8	10		
Unknown	1	0		
White	15	14		
Histological type			4.02439024	0.13369488
DLBCL, not otherwise specified (DLBCL, NOS)	21	20		
Primary DLBCL of the CNS (PCNSL)	0	3		
Primary mediastinal DLBCL (PMBCL)	3	1		

Next, we classified the patients into low and high expression groups according to the median AFAP1-AS1 expression levels in DLBCL tissues. Between the two groups, there were no differences in the clinical characteristics, including age, gender, race, and histological type (**Table 1**). The Kaplan-Meier survival analysis showed that patients with an AFAP1-AS1 expression that was high, had significantly poorer DFS (Hazard Ratio = 2.325) and OS (Hazard Ratio = 2.115) compared to those with a low expression (**Figure 1B**, **1C**). The observation of no statistical differences could be due to the limited sample size.

AFAP1-AS1 knockdown inhibited OCI-ly1 and OCI-ly19 cell proliferation

To evaluate the biological influence of AFAP1-AS1 on GCB-DLBCL cells, we constructed three AFAP1-AS1 shRNAs (sh-AFAP1-AS1#1, sh-AFAP1-AS1#2, and sh-AFAP1-AS1#3) and transduced them into OCI-ly1 and OCI-ly19 cells. All three constructs could decrease the expression of AFAP1-AS1 efficiently. The intervention efficiencies of the three shRNAs were about 60% in OCI-ly1 cells, indicating that all three specifically targeted AFAP1-AS1 (**Figure 1D**). We selected sh-AFAP1-AS1#3 as the representative AFAP1-AS1 shRNA in the subsequent assays.

To study the impact of silencing AFAP1-AS1 on proliferation of the cell, we performed CCK-8 assays 24, 48, 72, and 96 h following sh-AFAP1-AS1 adenovirus transduction. Compared to the sh-NC-transduced cells, cell proliferation of sh-AFAP1-AS1-transduced OCI-ly1 and OCI-ly19 cells was significantly inhibited at the 72 h and 96 h time points (**Figure 1E**, **1F**). These outcomes indicate that AFAP1-AS1 knockdown inhibited the proliferation of OCI-ly1 and OCI-ly19 cells.

AFAP1-AS1 knockdown prompts G0/G1 cell cycle arrest in OCI-ly1 and OCI-ly19 cells

To investigate the impact of AFAP1-AS1 knockdown on progression of the cell cycle, we evaluated the cell cycle distribution of OCI-ly1 and OCI-ly19 cells through flow cytometry. Our data showed that AFAP1-AS1 knockdown increased the G1 phase from 48.83 ± 4.53% to 61.56 ± 5.91% and 49.08 ± 4.84% to 65.46 ± 6.77% in sh-AFAP1-AS1-transduced OCI-ly1 and OCI-ly19 cells, respectively, compared to the sh-NC-transduced OCI-ly1 cells ($P < 0.05$) (**Figure 2A**, **2B**). The expression levels of Cyclin D1 and E1 protein also decreased significantly ($P < 0.05$) in the sh-AFAP1-AS1 cells in comparison to the sh-NC control cells (**Figure 2E**, **2F**). These outcomes indicate that AFAP1-AS1 knockdown in GCB-DLBCL cells led to arrest of the G0/G1 cell cycle.

AFAP1-AS1 knockdown induced apoptosis in OCI-ly1 and OCI-ly19 cells

Subsequently, we evaluated the relation amongst AFAP1-AS1 knockdown and apoptosis in OCI-ly1 and OCI-ly19 cells. In OCI-ly1 cells, the

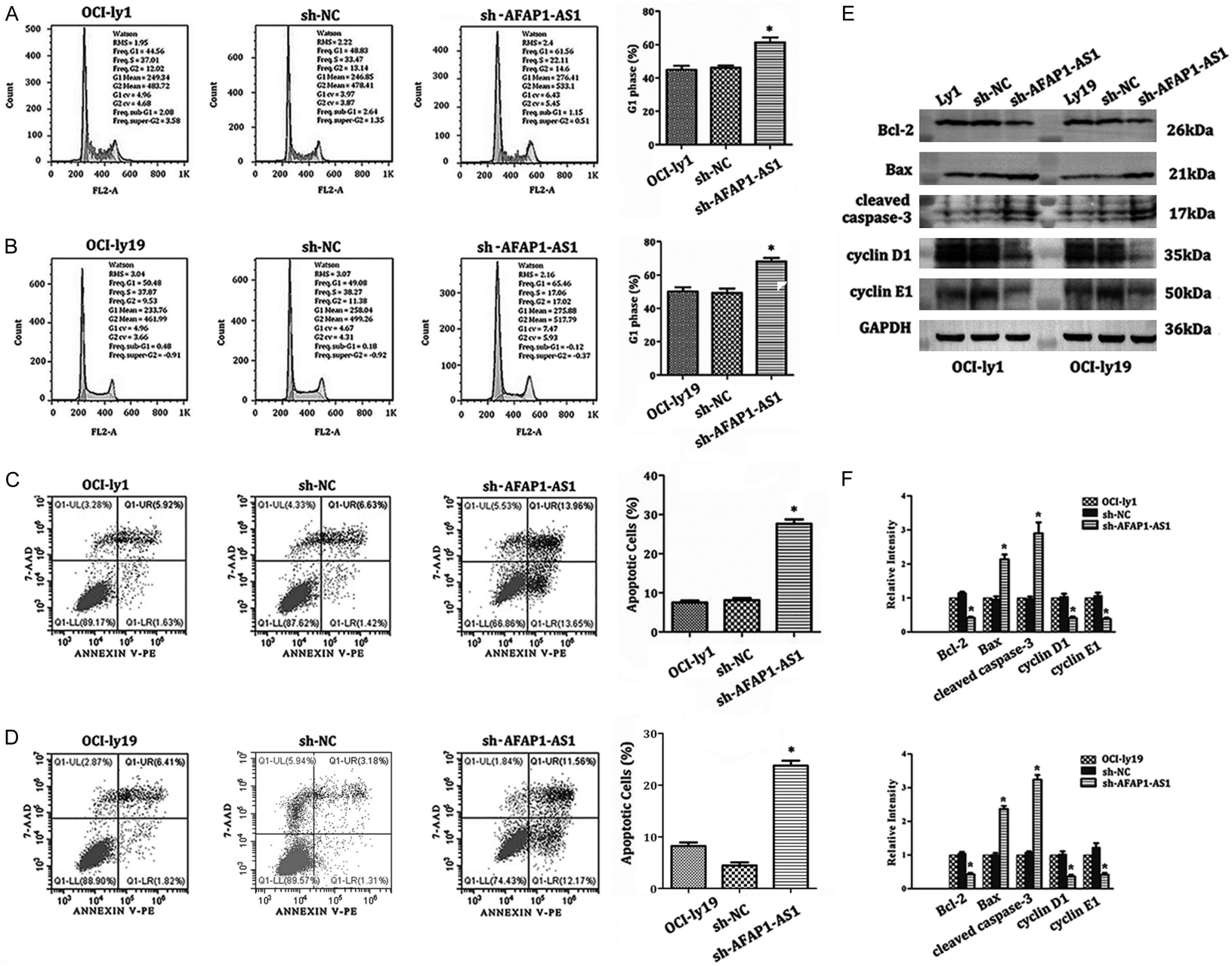
A
OCI-ly1
sh-NC
sh-AFAP1-AS1
Count
FL2-A
G1 phase (%)
OCI-ly1
sh-NC
sh-AFAP1-AS1
B
OCI-ly19
sh-NC
sh-AFAP1-AS1
C
OCI-ly1
sh-NC
sh-AFAP1-AS1
Q1-UL(3.28%)
Q1-UR(5.92%)
Q1-LL(89.17%)
Q1-LR(1.63%)
Q1-UL(4.33%)
Q1-UR(6.63%)
Q1-LL(87.62%)
Q1-LR(1.42%)
Q1-UL(5.53%)
Q1-UR(13.96%)
Q1-LL(66.86%)
Q1-LR(13.65%)
7-AAD
ANNEXIN V-PE
Apoptotic Cells (%)
D
OCI-ly19
sh-NC
sh-AFAP1-AS1
Q1-UL(2.87%)
Q1-UR(6.41%)
Q1-LL(88.90%)
Q1-LR(1.82%)
Q1-UL(5.94%)
Q1-UR(3.18%)
Q1-LL(89.57%)
Q1-LR(1.31%)
Q1-UL(1.84%)
Q1-UR(11.56%)
Q1-LL(74.43%)
Q1-LR(12.17%)
E
Ly1
sh-NC
sh-AFAP1-AS1
Ly19
sh-NC
sh-AFAP1-AS1
Bcl-2
26kDa
Bax
21kDa
cleaved caspase-3
17kDa
cyclin D1
35kDa
cyclin E1
50kDa
GAPDH
36kDa
OCI-ly1
OCI-ly19
F
OCI-ly1
sh-NC
sh-AFAP1-AS1
Relative Intensity
Bcl-2
Bax
cleaved caspase-3
cyclin D1
cyclin E1
OCI-ly19
sh-NC
sh-AFAP1-AS1

Figure 2. AFAP1-AS1 knockdown prompted arrest of the G0/G1 cell cycle and suppressed cell proliferation in OCI-ly1 and OCI-ly19 cells. Cell cycle distribution in OCI-ly1 (A) and OCI-ly19 cells (B) was detected by flow cytometry following sh-NC and sh-AFAP1-AS1 transduction. The apoptosis rate in OCI-ly1 (C) and OCI-ly19 cells (D) was detected by flow cytometry following sh-NC and sh-AFAP1-AS1 transduction. The expression levels of apoptosis and cell cycle-related proteins (cyclin D1, cyclin E1, cleaved-caspase3, Bax, and Bcl-2) in OCI-ly1 and OCI-ly19 cells were examined by western blotting following sh-NC and sh-AFAP1-AS1 transduction (E, F).

apoptotic rate of the sh-AFPA1-AS1-transduced OCI-ly1 and OCI-ly19 cells (27.61 ± 1.94% and 23.73 ± 1.79%, respectively) was higher compared to the sh-NC control cells (8.05 ± 1.03%, and 4.49% ± 1.01, respectively, $P < 0.05$) (**Figure 2C**, **2D**). In addition, cleaved caspase3 and Bax protein expression levels increased, while Bcl-2 levels decreased significantly ($P < 0.05$) in the sh-AFAP1-AS1-transduced cells in comparison to the sh-NC control cells (**Figure 2E**, **2F**). Thus, AFAP1-AS1 knockdown induced apoptosis in GCB-DLBCL cells.

Quantitative proteomics revealed the downstream proteins of AFAP1-AS1 in GCB-DLBCL

To study the downstream proteins of AFAP1-AS1, we performed label-free quantitative proteomics after the transduction of OCI-ly19 cells with sh-NC or sh-AFAP1-AS1 adenovirus. Our proteomics results revealed 122 upregulated and 124 downregulated proteins in sh-AFAP1-AS1-transduced OCI-ly19 cells compared to the sh-NC control cells (Fold change ≥ 2; Supplementary Table 2). Subsequently, we performed GO, KEGG pathway, and KOG function classification analysis for these deregulated proteins to identify the possible molecular mechanisms of AFAP1-AS1 in GCB-DLBCL.

The GO analysis revealed that the most enhanced GO terms associated with the upregulated proteins included “cellular process” (ontology: biological process), “cell” (ontology: cellular component), and “binding” (ontology: molecular function), which were the same for the downregulated proteins (**Figure 3A**). The KEGG pathway analysis revealed that the differentially expressed proteins were correlated to multiple signaling pathways. “RNA transport”, which included three upregulated proteins and four downregulated proteins in our profiles, was the most enriched pathway (**Figure 3B**). The enrichment scores of the GO and KEGG terms are presented in **Figure 4A**, **4B**). Additionally, the deregulated proteins were also enriched in several pathways associated with tumors, such as “ubiquitin-mediated proteolysis”, the “NOD-like receptor signaling pathway”, the “B-cell receptor signaling pathway”, the “TNF signaling pathway”, and “autophagy”. Furthermore, the proteins were compared to the KOG database to estimate and categorize potential functions. A total of 246 proteins (122 upregulated proteins and 124 downregulated proteins) were assigned to 24 terms. The KOG function classification analysis showed that the most enriched terms included “transcription” (category: information storage and processing), “signal transduction mechanisms” (category: cellular processes and signaling), “energy production and conversation” (category: metabolism), and “general function prediction only” (category: poorly characterized) (**Figure 4C**).

Because the deregulated proteins resulting from AFAP1-AS1 knockdown were enriched in several pathways associated with tumors, we selected the B-cell receptor and TNF signaling pathways for further study to validate their critical roles in GCB-DLBCL (**Figure 5A**). The deregulated proteins and their fold-changes were shown in Supplementary Table 2. Similar to the proteomics results, western blotting revealed that the expression levels of key members of these pathways (BTK, p-BTK, and DRP1) were significantly decreased ($P < 0.05$) in the sh-AFAP1-AS1-transduced cells in comparison to the sh-NC control cells (**Figure 5B-D**). These outcomes suggested that AFAP1-AS1 might exert its oncogenic ability in GCB-DLBCL by regulating the B-cell receptor and TNF signaling pathways.

ChIRP-MS identified proteins specifically bind to AFAP1-AS1 in OCI-ly19 cells

It has been shown that AFAP1-AS1 is mainly localized in the cytoplasm rather than the nucleus [18], consistent with the information presented in the RNALocate database (http://www.rna-society.org/rnalocate/), which suggests that AFAP1-AS1 might modulate gene expression at the post-transcriptional level. To investigate the proteins binding to AFAP1-AS1 in GCB-DLBCL, we performed ChIRP-MS experi-

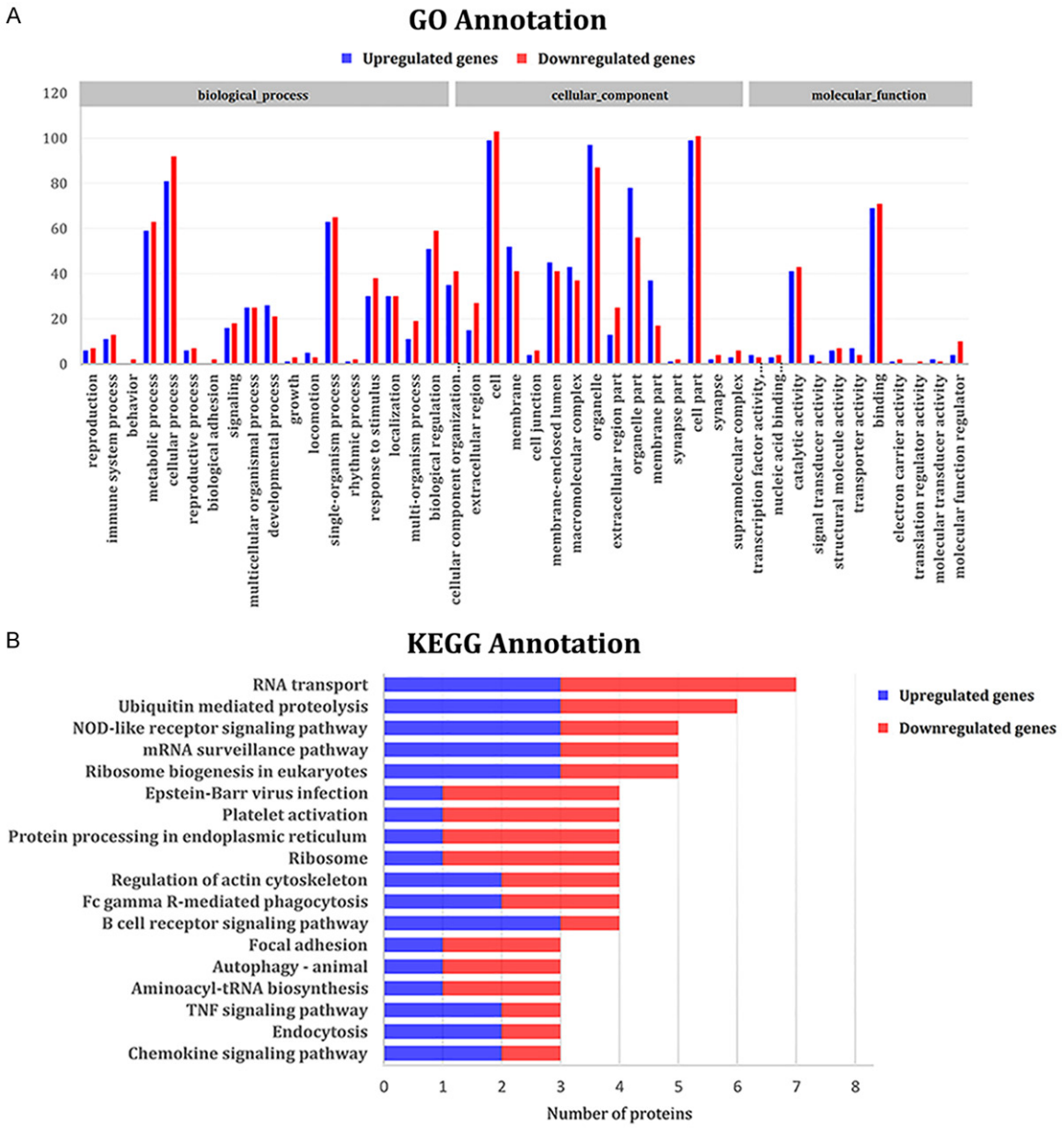

Figure 3. Quantitative proteomics revealed the downstream proteins of AFAP1-AS1 in GCB-DLBCL. GO (A) and KEGG (B) annotation of the differentially expressed proteins after knockdown of AFAP1-AS1 in OCI-ly19.

ments in OCI-ly19 cells. The ChIRP-MS results showed that 103 proteins could specifically bind to AFAP1-AS1 in the OCI-ly19 cells (Supplementary Table 3). Subsequently, we performed GO, KEGG pathway, and protein-protein interaction analysis for these binding proteins. The GO analysis revealed that the most enhanced GO terms were: "mRNA catabolic process" (ontology: biological process), "focal adhesion" (ontology: cellular component), and "cell adhesion molecule binding" (ontology: molecular function) (**Figure 6A**). The KEGG pathway analysis indicated that "ribosome" was the most enriched pathway (**Figure 6B**). To evaluate the protein interactions of these specific binding proteins we used the STRING database. Based on this analysis, 46 molecules had significantly enriched interactions (**Figure 6C**).

Alternative splicing is a crucial part of regulation on a post-transcriptional level. Indeed, we discovered by ChIRP-MS that several proteins (e.g., SFPQ, RBMX, SRSF2, KHSRP, SRSF6, and

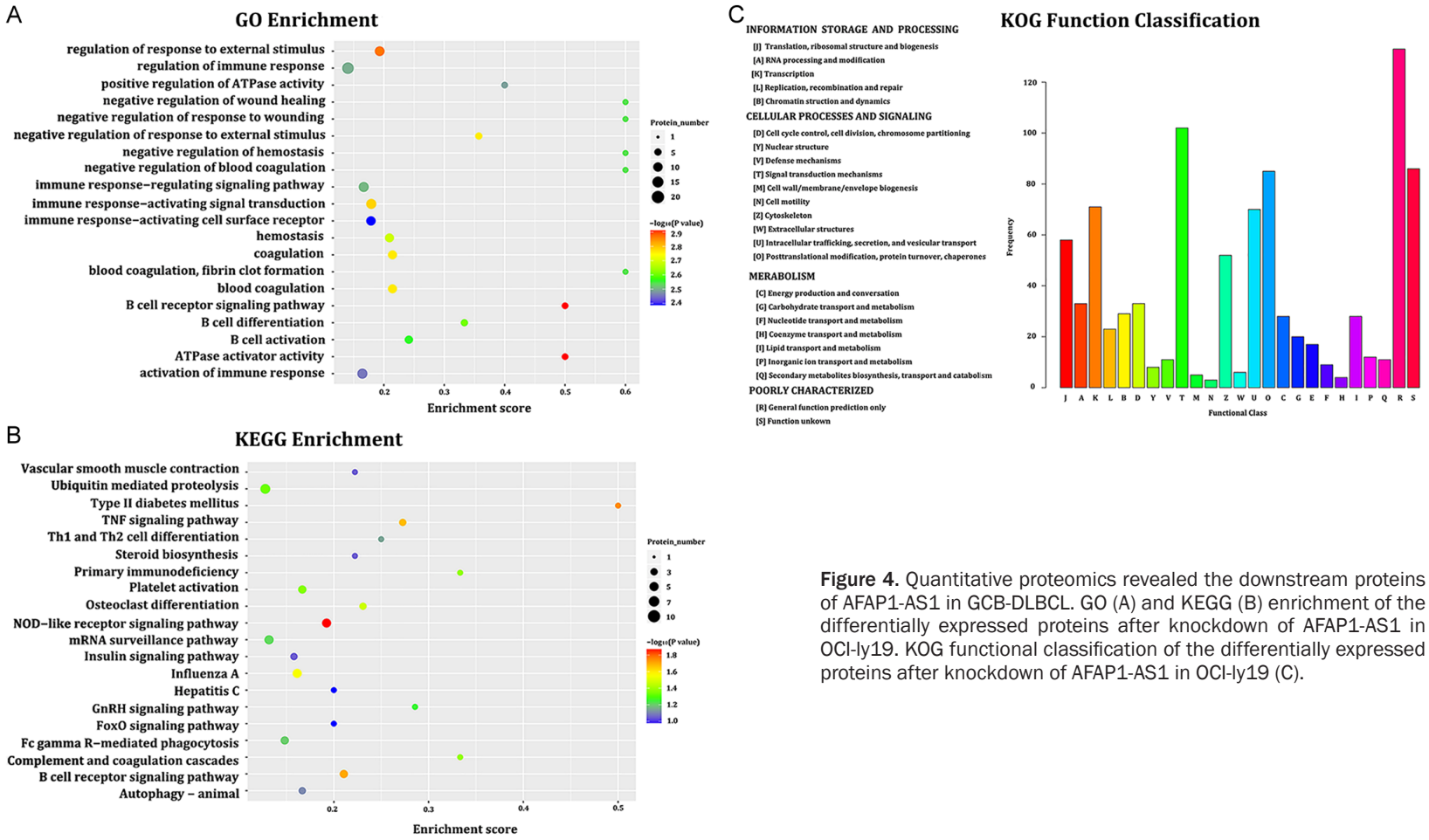

Figure 4. Quantitative proteomics revealed the downstream proteins of AFAP1-AS1 in GCB-DLBCL. GO (A) and KEGG (B) enrichment of the differentially expressed proteins after knockdown of AFAP1-AS1 in OCI-ly19. KOG functional classification of the differentially expressed proteins after knockdown of AFAP1-AS1 in OCI-ly19 (C).

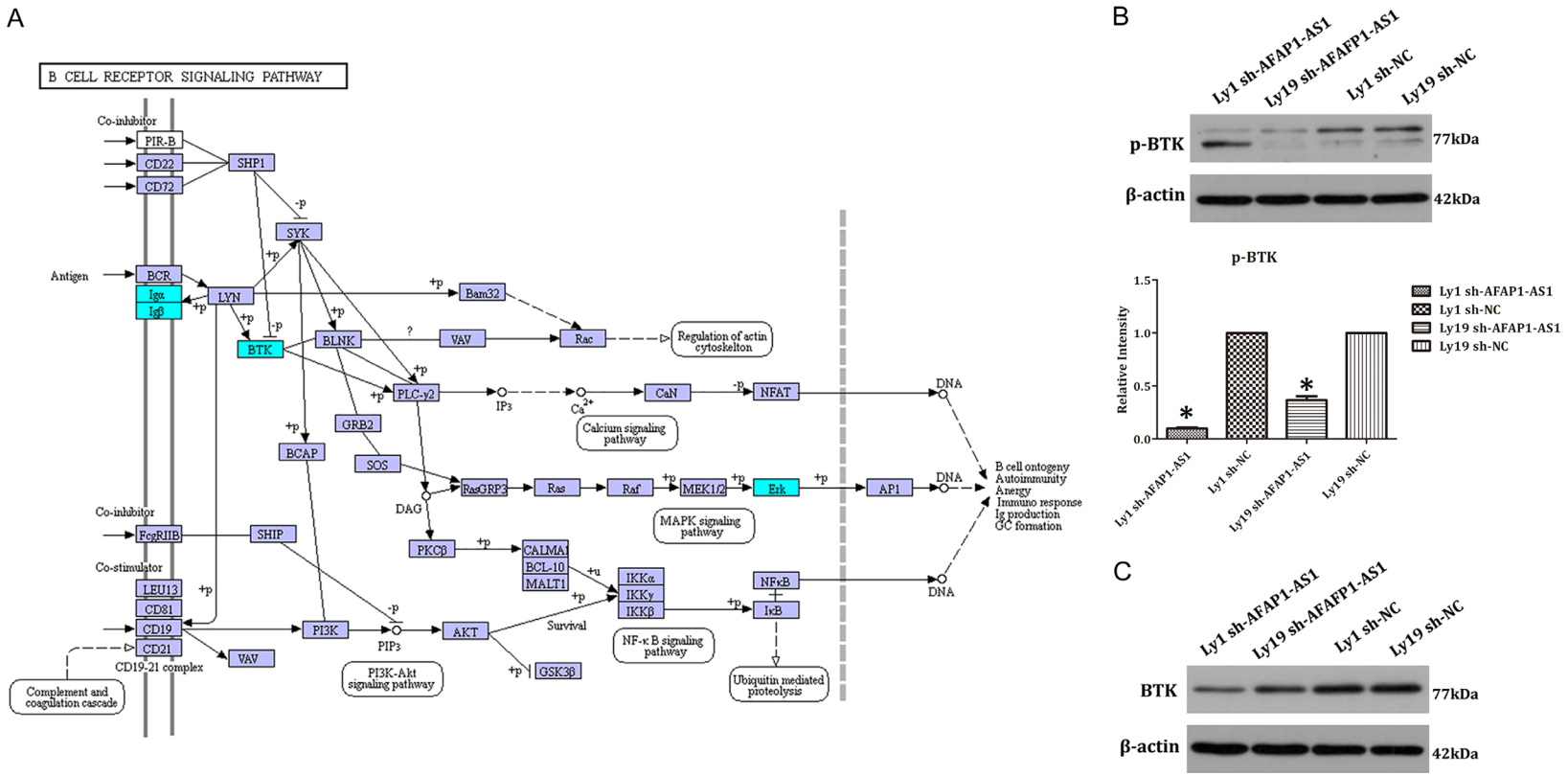
A
B CELL RECEPTOR SIGNALING PATHWAY
Co-inhibitor
PIR-B
CD22
CD72
SHP1
SYK
Antigen
BCR
Igα
Igβ
LYN
Bam32
BTK
BLNK
VAV
Rac
Regulation of actin cytoskelton
PLC-γ2
IP3
Ca2+
CaN
NFAT
DNA
Calcium signaling pathway
GRB2
BCAP
SOS
RasGRP3
Ras
Raf
MEK1/2
Erk
AP1
DNA
B cell ontogeny
Autoimmunity
Anergy
Immuno response
Ig production
GC formation
DAG
MAPK signaling pathway
Co-inhibitor
FcgRIIB
SHIP
PKCβ
CALMA1
BCL-10
MALT1
Co-stimulator
LEU13
CD81
CD19
CD21
CD19-21 complex
VAV
PI3K
PIP3
AKT
Survival
IKKα
IKKγ
IKKβ
NFκB
IκB
NF-κ B signaling pathway
GSK3β
PI3K-Akt signaling pathway
Ubiquitin mediated proteolysis
Complement and coagulation cascade
B
Ly1 sh-AFAP1-AS1
Ly19 sh-AFAFP1-AS1
Ly1 sh-NC
Ly19 sh-NC
p-BTK
77kDa
β-actin
42kDa
p-BTK
Relative Intensity
1.5
1.0
0.5
0.0
Ly1 sh-AFAP1-AS1
Ly1 sh-NC
Ly19 sh-AFAP1-AS1
Ly19 sh-NC
C
Ly1 sh-AFAP1-AS1
Ly19 sh-AFAP1-AS1
Ly1 sh-NC
Ly19 sh-NC
BTK
77kDa
β-actin
42kDa

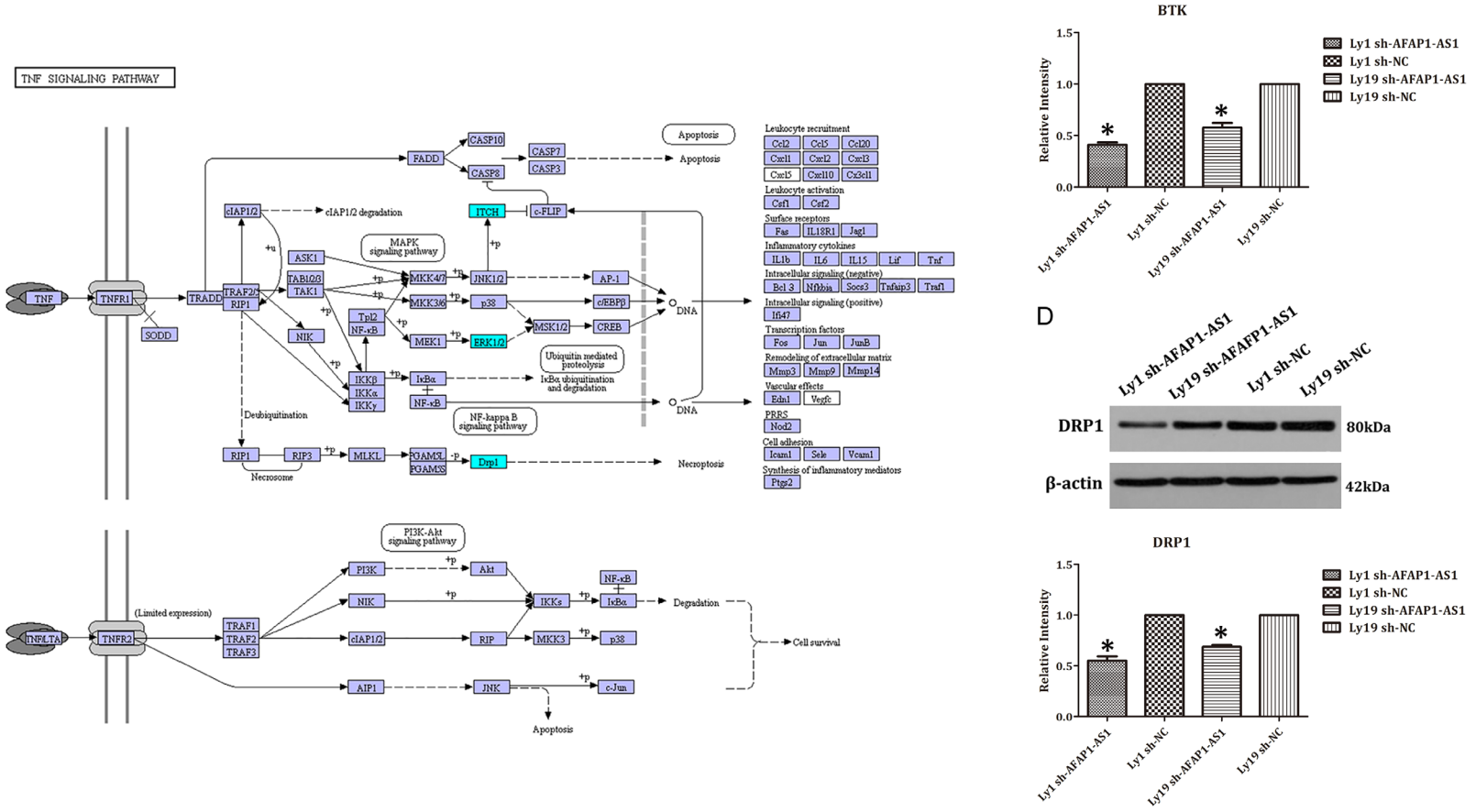

Figure 5. Validation of the results of quantitative proteomics. The deregulated proteins in the B-cell receptor and TNF signaling pathways (A). Confirmation of the BTK, p-BTK, and DRP1 expression levels in OCI-ly1 and OCI-ly19 cells by western blotting following transduction with sh-NC and sh-AFAP1-AS1 (B-D).

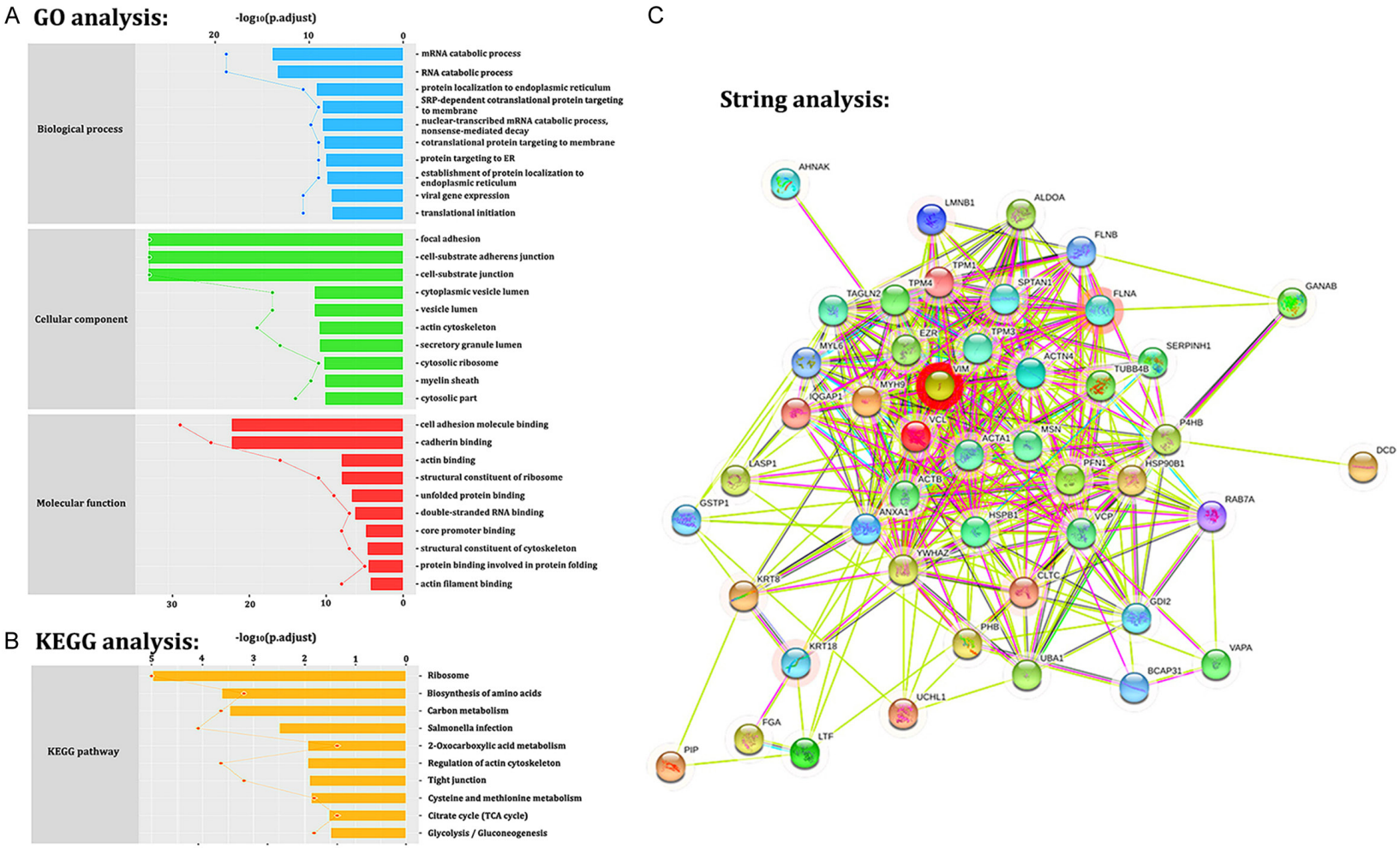

Figure 6. ChIRP-MS identified the proteins specifically binding to AFAP1-AS1 in OCI-ly19 cells. GO (A), KEGG (B), and protein-protein interaction (C) analysis for the proteins specifically binding to AFAP1-AS1 in OCI-ly19 cells.

Table 2. Identification and quantification of proteins binding to AFAP1-AS1 in the ChIRP experiment by MS and validation their quantification by PRM

Protein Name	ChIRP-MS		PRM		
	Unique Peptides	Fold Change (LNC/CON)	CON	LNC	Fold Change (LNC/CON)
VCP	6	1.047787899	2236962	3771598	1.686035793
CCT2	7	1.047787899	1309743	4999571	3.817215286
GOT2	3	1.159644801	2877170	6385967	2.21953065
P4HB	4	1.159644801	260573	2599825	9.977338404
SFPQ	5	1.159644801	813324	5030676	6.185328356
MSN	5	1.159644801	560076	810084	1.446382277
RBMX	11	1.159644801	1468404	8138370	5.542323502
TUFM	5	1.159644801	2628628	8311978	3.16209749
DCD	6	1.222926259	46329658	165634042	3.575119031
CCT6A	6	1.236560913	2500452	6481045	2.591949376
EZR	5	1.415504618	2773152	4004513	1.444029393
PFN1	5	1.415504618	3304332	16560047	5.011617174
TXNDC5	2	1.451026002	167318	1450301	8.667931723
UBA1	2	1.451026002	1142833	5749899	5.031267911
LASP1	2	1.451026002	1047166	6186433	5.907786349
SERPINH1	2	1.451026002	0	5318302	∞
SRSF2	3	1.451026002	3469859	7735181	2.229249373
EIF4A3	3	1.451026002	638083	3069737	4.810874134
IQGAP1	2	1.451026002	398277	2381105	5.978514953
KHSRP	4	1.451026002	1525244	6759147	4.431518498
PSMB1	2	1.451026002	5018564	5060948	1.008445444
RAB7A	2	1.451026002	1311573	5037408	3.840737801
SRSF6	4	1.451026002	2184727	9126744	4.177521494
RUVBL2	2	1.451026002	1736219	5709866	3.288678444
GDI2	2	1.451026002	3408285	6706850	1.967807856
LAP3	2	1.451026002	250250	2485653	9.932679321
GSTP1	3	1.451026002	312286	4999477	16.00928956
BCAP31	2	1.451026002	557218	1771005	3.17829826
LMNB2	2	1.451026002	5122043	10920353	2.132030715
HNRNPA0	2	1.451026002	179331	2558224	14.2653752
TPM3	5	1.553050599	233435	2939685	12.59316298
PGK1	8	1.617199396	2586057	11642220	4.501919331
ACTN4	7	1.6327504	937844	10951984	11.67783128
PHB	6	1.6327504	3376977	7889111	2.336145908
MATR3	6	1.84841213	432329	2812129	6.504604133
NONO	2	1.84841213	998907	5425208	5.431144241
UCHL1	2	1.84841213	289997	1725425	5.949802929
GANAB	3	1.84841213	2337947	2582117	1.104437782
XRCC5	4	1.84841213	0	2039708	∞
DHX9	4	1.84841213	290611	3725963	12.82113547
CCT7	3	1.84841213	0	321962	∞
VCL	8	1.988429608	1024510	9587624	9.358253214
MYH9	19	2.053651604	1347135	7663641	5.688844102
ANXA1	4	2.159644801	1189401	5164597	4.342183166
HNRNPU	9	2.273533927	4129724	19536988	4.730821721

LMNB1	10	2.397410477	358637	3397808	9.474226028
CLTC	6	2.821523413	937422	5783116	6.169170342
KRT18	5	3.1380131	1257364726	796563413	0.63351818
FLNA	16	4.127074392	166612	3795258	22.77901952
MAGEA4	2	1.451026002	207842	1271800	6.119071218

NONO) associated with RNA splicing, specifically bound to AFAP1-AS1 in OCI-ly19 cells (**Table 2**), suggesting that AFAP1-AS1 could promote GCB-DLBCL tumor progression through binding to these specific proteins.

To verify the ChIRP-MS results, we performed PRM assay and validated 50 selected proteins. The extracted ion chromatograms (XIC) showed that the intensity and retention time of each fragment ion related to the prospective peptides of proteins associated with RNA splicing (SFPQ, RBMX, SRSF2, KHSRP, SRSF6, and NONO) in the LNC group, and the histograms present the quantitative comparison of the prospective peptides between the sample groups (**Figure 7**). The different colors represent different fragment ions of the same peptide, which have the same chromatographic peak type, indicating that this peptide was identified in the LNC group. Compared to the ChIRP-MS results, the levels of relative expression of most of the selected proteins followed the same tendencies (**Table 2**). Thus, the data on PRM additionally validated the authenticity of the ChIRP-MS findings. The PRM results of the remaining 44 proteins are shown in the Supplementary Figures 1, 2 and 3.

Discussion

In the past few years, the rapid progress of high-throughput technology has aided the identification of genetic lesions in GCB-DLBCL. GCB-DLBCL is characterized by chromosome aberrations, such as t(14;18)(q32;q21) [2], 10q23 deletion [19, 20], and somatic mutations associated with chromatin remodeling (e.g., acquired functional mutation of EZH2 and inactivating mutations or deletions of MLL2, CREBBP, or EP300 gene) [21-24]. Accumulating data has demonstrated the critical roles of lncRNAs in various malignancies. In our previous study, we used microarray analysis to explore the lncRNA expression profiles in GCB-DLBCL [8]. Here, we selected one of the most upregulated lncRNAs, AFAP1-AS1, for additional study. AFAP1-AS1 was identified and reported for the first time in Barrett's esophagus and esophageal adenocarcinoma as exceedingly hypomethylated and overexpressed [10]. Many subsequent research has confirmed that AFAP1-AS1 is associated with oncogenesis and tumor progression, and may be a novel biomarker for prognosis and diagnosis prediction [16, 18, 25]. However, the role of AFAP1-AS1 in GCB-DLBCL is unknown.

In the present study, we demonstrated that AFAP1-AS1 was a potential marker of prognosis for predicting poor outcomes in GCB-DLBCL patients because patients, whose AFAP1-AS1 expression was high, had a significantly poorer DFS and OS. Furthermore, we clarified the biological function of AFAP1-AS1 in GCB-DLBCL. Specifically, we showed that AFAP1-AS1 functions in cell proliferation and the cell cycle's G1 phase, and prevented apoptosis in GCB-DLBCL cell lines.

LncRNA's mechanisms are largely dependent on their position in cells. If a lncRNA is located in the nucleus, its main mechanism is to regulate the chromatin state and transcription; if a lncRNA is located inside the cytoplasm, then it functions as a contending endogenous RNA (ceRNA) or participates in post-transcriptional regulation, such as mRNA alternative splicing, mRNA stability, and subcellular localization regulation. AFAP1-AS1 was previously shown to be mainly distributed in the cytoplasm rather than the nucleus [18], consistent with the information presented in the RNALocate database. Multiple research has demonstrated that AFAP1-AS1 can act as a ceRNA of microRNAs to facilitate tumor progression [17, 25-27]. However, there is less information available on the exact regulatory mechanism of AFAP1-AS1 directly interacting with proteins. Recently, Han et al. [18] showed that AFAP1-AS1 was able to promote the resistance of trastuzumab by binding to AUF1 and activating the translation of ERBB2. Yu et al. [16] found that AFAP1-AS1 promoted non-small cell lung cancer progression by binding to LSD1 and inhibiting HBP1.

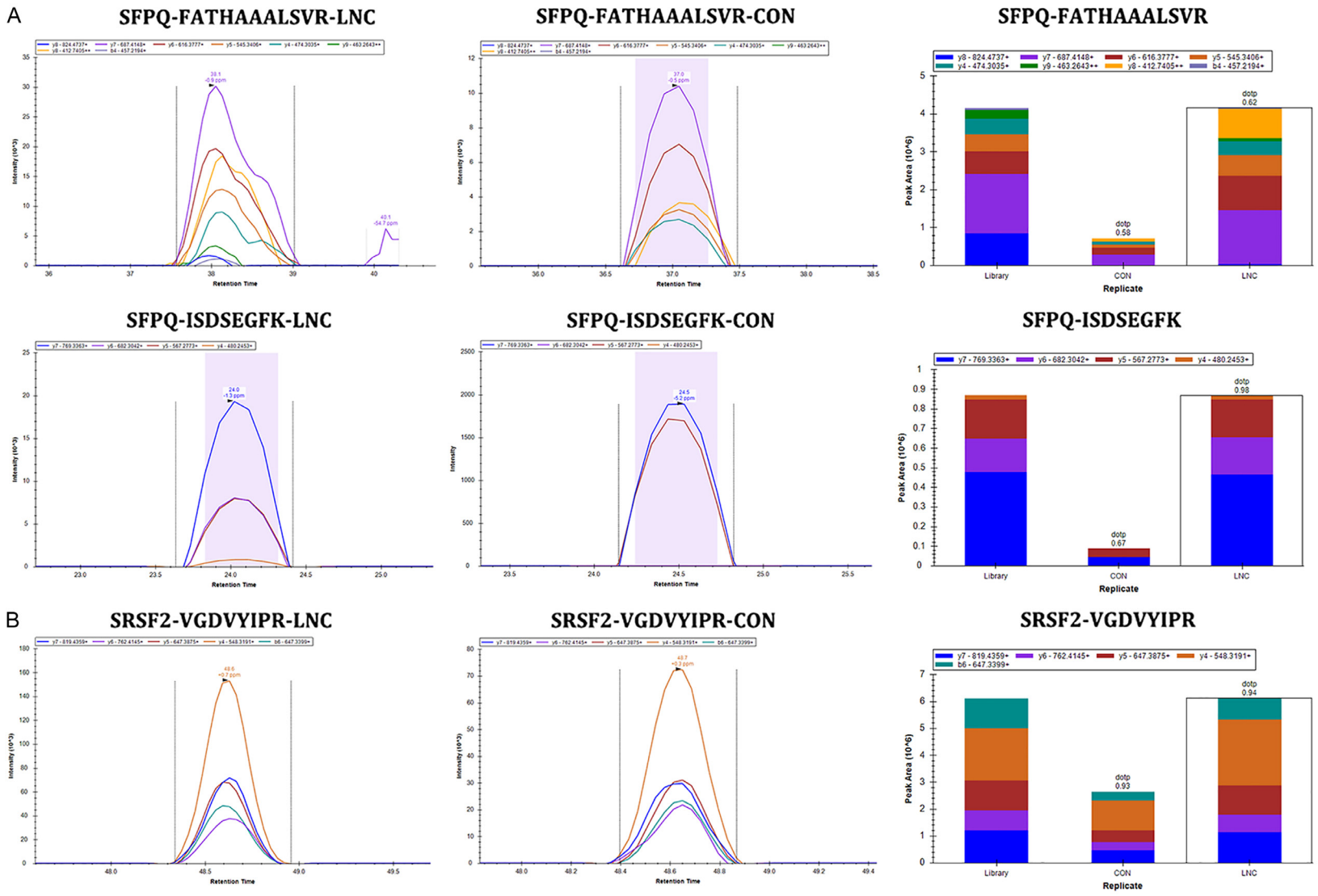
A
SFPQ-FATHAAALSVR-LNC
SFPQ-FATHAAALSVR-CON
SFPQ-FATHAAALSVR
SFPQ-ISDSEGFK-LNC
SFPQ-ISDSEGFK-CON
SFPQ-ISDSEGFK
B
SRSF2-VGDVYIPR-LNC
SRSF2-VGDVYIPR-CON
SRSF2-VGDVYIPR
Retention Time
Peak Area (10^6)
Library
CON
LNC
Replicate
dotp 0.62
dotp 0.58
dotp 0.98
dotp 0.67
dotp 0.94
dotp 0.93

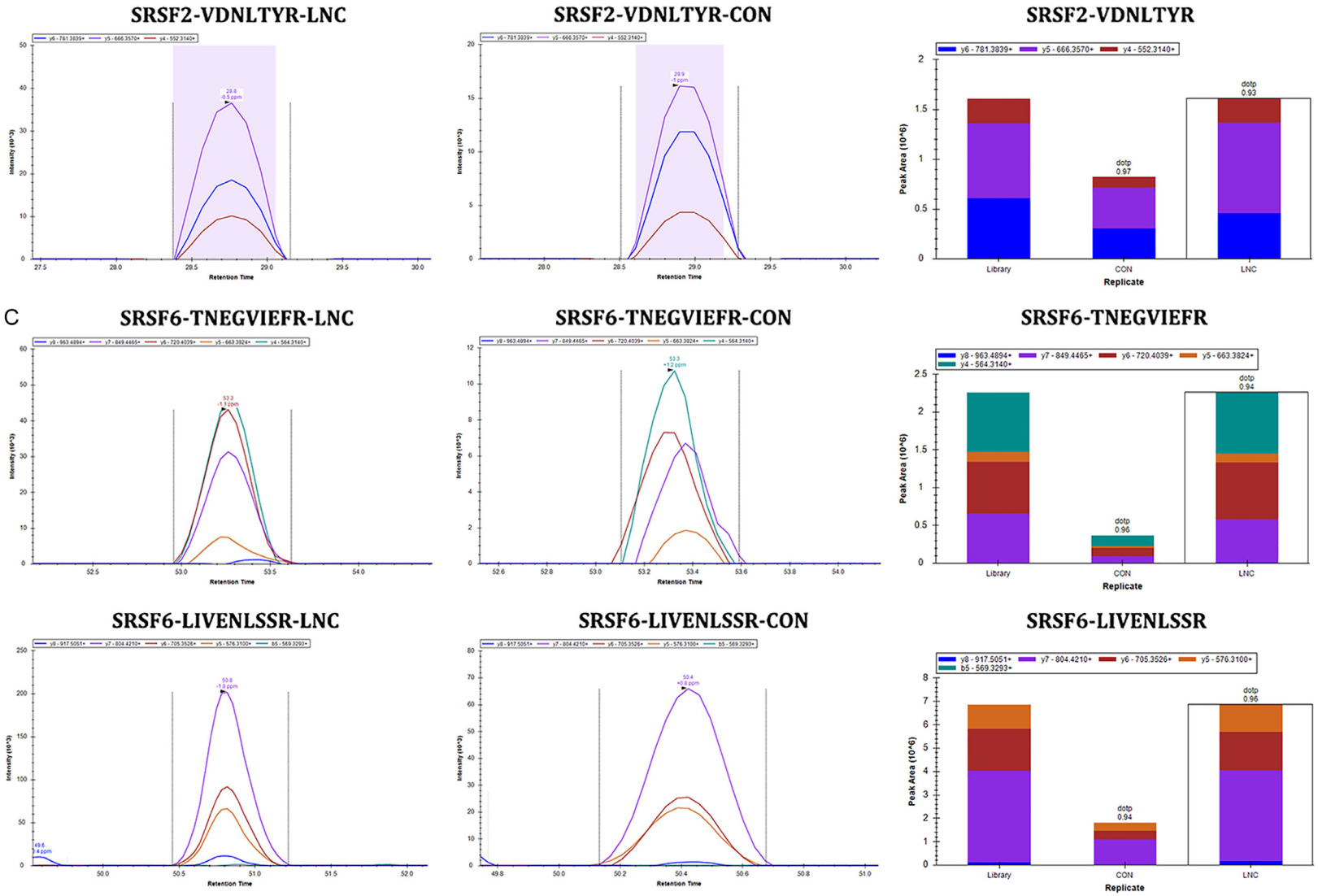
SRSF2-VDNLTYR-LNC
SRSF2-VDNLTYR-CON
SRSF2-VDNLTYR
y6 - 781.3839+
y5 - 666.3570+
y4 - 552.3140+
Intensity (10^3)
Retention Time
Peak Area (10^6)
dotp 0.93
dotp 0.97
Library
CON
LNC
Replicate
C
SRSF6-TNEGVIEFR-LNC
SRSF6-TNEGVIEFR-CON
SRSF6-TNEGVIEFR
y8 - 963.4894+
y7 - 849.4465+
y6 - 720.4039+
y5 - 663.3824+
y4 - 564.3140+
dotp 0.94
dotp 0.96
SRSF6-LIVENLSSR-LNC
SRSF6-LIVENLSSR-CON
SRSF6-LIVENLSSR
y8 - 917.5051+
y7 - 804.4210+
y6 - 705.3526+
y5 - 576.3100+
b5 - 569.3293+
dotp 0.96
dotp 0.94

D

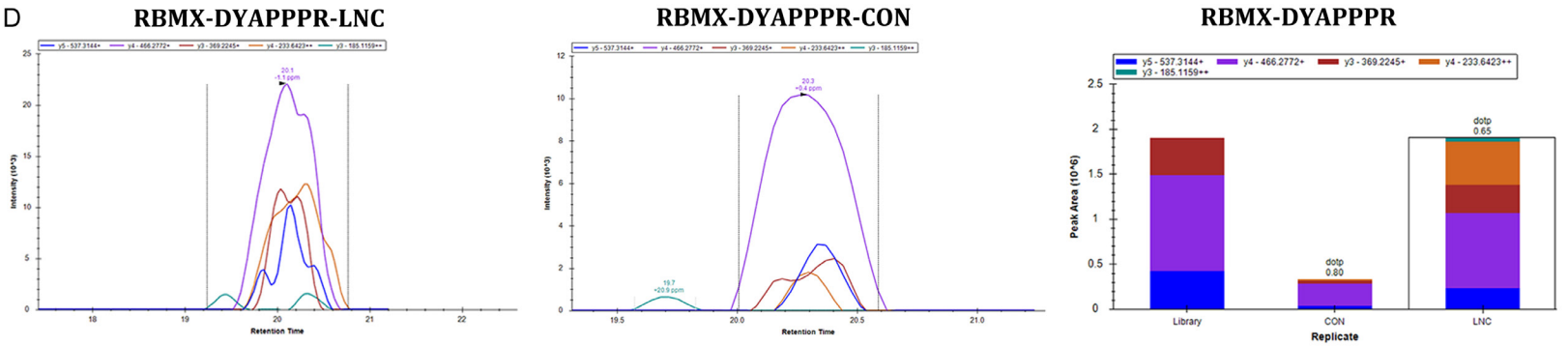
RBMX-DYAPPPR-LNC
RBMX-DYAPPPR-CON
RBMX-DYAPPPR
y5 - 537.3144+
y4 - 466.2772+
y3 - 369.2245+
y4 - 233.6423++
y3 - 185.1159++
Retention Time
Peak Area (10^6)
dotp 0.80
dotp 0.65
Library
CON
LNC
Replicate

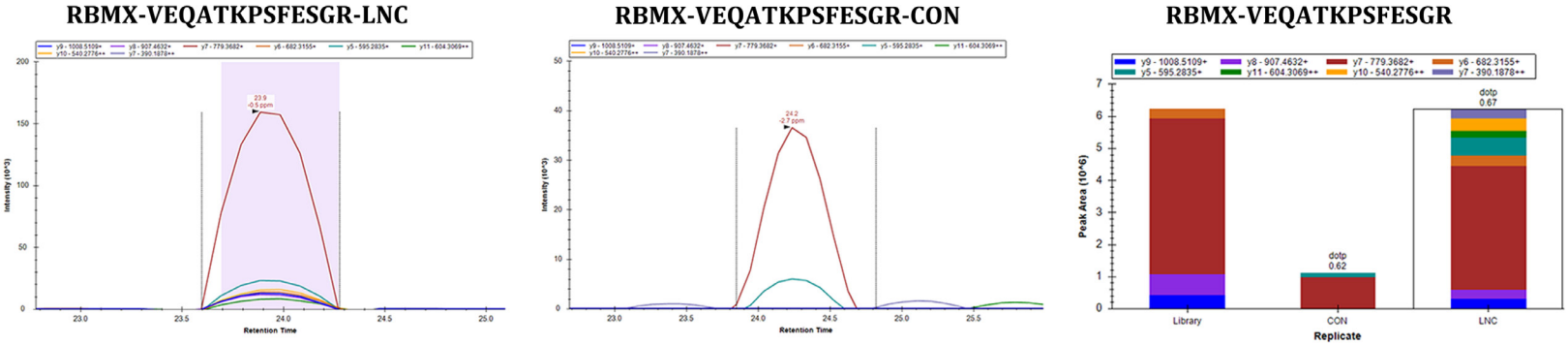
RBMX-VEQATKPSFESGR-LNC
RBMX-VEQATKPSFESGR-CON
RBMX-VEQATKPSFESGR
y9 - 1008.5109+
y8 - 907.4632+
y7 - 779.3682+
y6 - 682.3155+
y5 - 595.2835+
y11 - 604.3069++
y10 - 540.2776++
y7 - 390.1878++
Retention Time
Peak Area (10^6)
dotp 0.62
dotp 0.67
Library
CON
LNC
Replicate

E

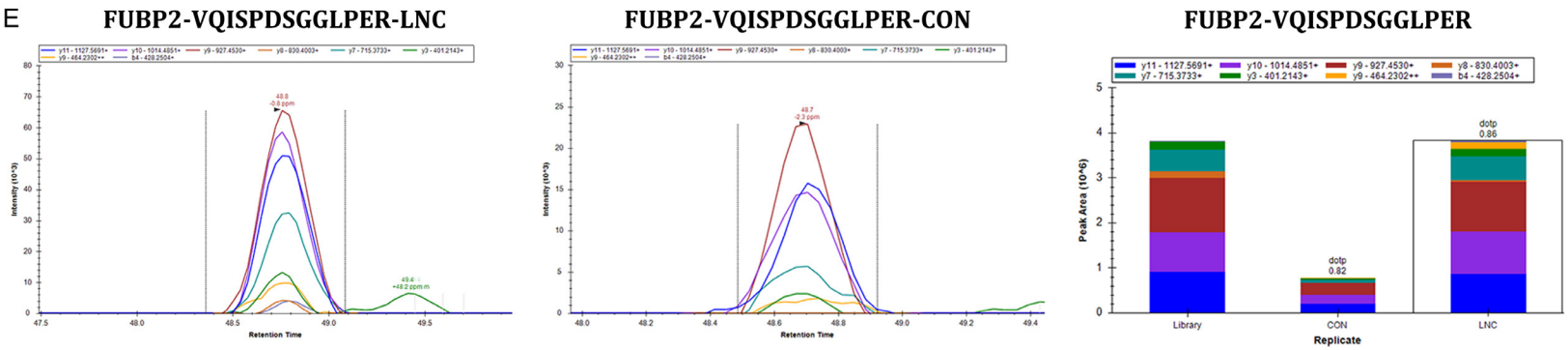
FUBP2-VQISPDSGGLPER-LNC
FUBP2-VQISPDSGGLPER-CON
FUBP2-VQISPDSGGLPER
y11 - 1127.5691+
y10 - 1014.4851+
y9 - 927.4530+
y8 - 830.4003+
y7 - 715.3733+
y3 - 401.2143+
y9 - 464.2302++
b4 - 428.2504+
Retention Time
Peak Area (10^6)
dotp 0.82
dotp 0.86
Library
CON
LNC
Replicate

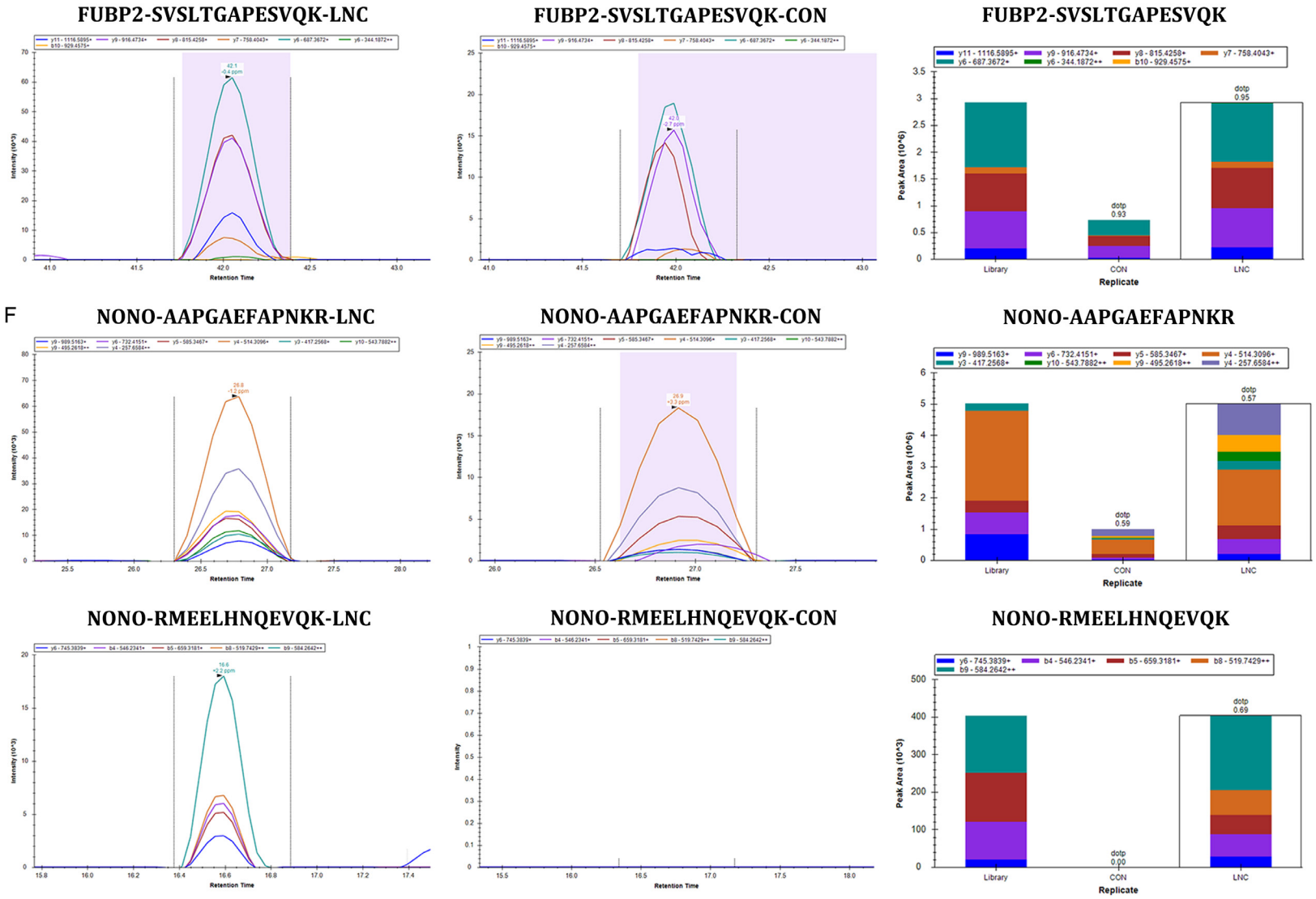

Figure 7. Validation of ChIRP-MS results by PRM. Extracted ion chromatograms for the retention time and intensity of each fragment ion corresponding to the peptides of SFPQ, RBMX, SRSF2, KHSRP, SRSF6, and NONO in the LNC group. Histograms for the quantitative comparison of the peptides between the sample groups.

To analyze the modulatory mechanism of AFAP1-AS1 in GCB-DLBCL, we conducted ChIRP-MS experiments in OCI-ly19 cells. It is generally known that some lncRNAs can competitively bind to the RISC complex, which consists of Dicer enzyme, AGO protein (mainly AGO2), and microRNA, to reduce the degradation of microRNA on its target genes (i.e., ceRNA mechanism). If AFAP1-AS1 acts as a molecular sponge in GCB-DLBCL, two conditions are required for AFAP1-AS1: cytoplasmic localization and binding to the AGO protein. However, no AGO protein was bound to AFAP1-AS1 according to the ChIRP-MS results, implying that AFAP1-AS1 did not function through a ceRNA mechanism in GCB-DLBCL. Thus, we proposed that AFAP1-AS1 participated in post-transcriptional regulation in GCB-DLBCL, such as mRNA alternative splicing or mRNA stability regulation. Interestingly, we discovered several proteins (e.g., SFPQ, NONO, SRSF2, SRSF6, and KHSRP) associated with RNA splicing that could specifically bind to AFAP1-AS1 in OCI-ly19 cells.

At first, SFPQ was recognized as a protein needed in pre-mRNA splicing and located in the nucleoplasm, nucleolar caps, and paraspeckles [28]. Paraspeckles consist of lncRNA NEAT1 and elements of protein, such as SFPQ, NONO, and PSPC1. LcRNA SANT1 can cis-regulate the expression of SLC47A2 by detaching the regulatory SFPQ/E2F1/HDAC1 suppressor complex from its promoter region in renal cell carcinoma, which significantly increases the amount of RNAPII binding and H3K27ac modifications [29]. Additionally, lncRNA MALAT1 can promote the metastasis and cell proliferation of colorectal carcinoma through binding to the tumor inhibiting gene SFPQ and releasing the oncogene PTBP2 from the SFPQ/PTBP2 complex [30]. Wang et al. [31] found that NEAT1 paraspeckles could promote STAT3 phosphorylation, induced by IL-6, through binding and keeping PRDX5 mRNA in the nucleus and lowering PRDX5 protein levels. Thus, there is less PRDX5 that can engage with STAT3 directly and suppress its phosphorylation, resulting in accelerated hepatocellular carcinoma progression.

Ser/Arg-rich (SR) proteins are directly involved in the regulation of tumor development acting as splicing regulators [32-34]. SRSF2 and SRSF6 are members of the SR protein family and the LncRNA AC091729.7 can promote growth and invasion of sinonasal squamous cell carcinoma by connecting to SRSF2 [35]. Moreover, LINC01133 suppresses metastasis and the epithelial-mesenchymal transition in colorectal carcinoma through removing SRSF6 from its target RNAs [36].

KHSRP, part of the RBP family, can bind to AU-rich components in the 3'UTR regions of its targeted mRNAs, and promote decay of the mRNA [37, 38]. Gou et al. [39] showed that lncRNA AB074169 overexpression resulted in arrest of the cell cycle and inhibited growth of the tumor in papillary thyroid carcinoma. Mechanistic analyses demonstrated that lncAB, connected to KHSRP, and subsequently to the 3'UTR region of p21 mRNA, resulted in decreased p21 mRNA decay and increased p21 expression, which repressed cell proliferation.

In conclusion, our study showed that the lncRNA AFAP1-AS1 could modulate the expression of genes through binding to specific proteins (e.g., SFPQ, NONO, SRSF2, SRSF6, and KHSRP) to promote cell cycle progression, cell growth, and inhibit apoptosis in GCB-DLBCL. Our findings have provided understanding of the development and manifestation of GCB-DLBCL and a potential prognostic biomarker for this disease. Moreover, our ChIRP-MS results may still have reference values for the mechanism study of AFAP1-AS1 in other diseases. However, some aspects of our research require improvement. Although our bioinformatics analysis showed that GCB-DLBCL patients with a high expression of AFAP1-AS1 had a poor outcome, there was no statistical difference, presumably due to the small sample size. Thus, our results need to be validated in a larger clinical population. More elaborate mechanisms for AFAP1-AS1 in GCB-DLBCL will be explored in future studies.

Acknowledgements

This study was supported by the Natural Science Foundation of Liaoning Province (20180550879), 2019 Xisike-Roche Oncology Research Fund, and the 345 Talent Project of Shengjing Hospital Affiliated to the China Medical University.

Disclosure of conflict of interest

None.

Address correspondence to: Wei Yang, Department of Hematology, Shengjing Hospital Affiliated to China Medical University, 39 Huaxiang Road, Tiexi, Shenyang 110000, Liaoning, P. R. China. E-mail: yangwei_sj@163.com

References

[1] Rodriguez-Abreu D, Bordoni A and Zucca E. Epidemiology of hematological malignancies. Ann Oncol 2007; 18 Suppl 1: i3-i8.

[2] Iqbal J, Sanger WG, Horsman DE, Rosenwald A, Pickering DL, Dave B, Dave S, Xiao L, Cao K, Zhu Q, Sherman S, Hans CP, Weisenburger DD, Greiner TC, Gascoyne RD, Ott G, Muller-Hermelink HK, Delabie J, Braziel RM, Jaffe ES, Campo E, Lynch JC, Connors JM, Vose JM, Armitage JO, Grogan TM, Staudt LM and Chan WC. BCL2 translocation defines a unique tumor subset within the germinal center B-cell-like diffuse large B-cell lymphoma. Am J Pathol 2004; 165: 159-166.

[3] Morin RD, Johnson NA, Severson TM, Mungall AJ, An J, Goya R, Paul JE, Boyle M, Woolcock BW, Kuchenbauer F, Yap D, Humphries RK, Griffith OL, Shah S, Zhu H, Kimbara M, Shashkin P, Charlot JF, Tcherpakov M, Corbett R, Tam A, Varhol R, Smailus D, Moksa M, Zhao Y, Delaney A, Qian H, Birol I, Schein J, Moore R, Holt R, Horsman DE, Connors JM, Jones S, Aparicio S, Hirst M, Gascoyne RD and Marra MA. Somatic mutations altering EZH2 (Tyr641) in follicular and diffuse large B-cell lymphomas of germinal-center origin. Nat Genet 2010; 42: 181-185.

[4] Morin RD, Mendez-Lago M, Mungall AJ, Goya R, Mungall KL, Corbett RD, Johnson NA, Severson TM, Chiu R, Field M, Jackman S, Krzywinski M, Scott DW, Trinh DL, Tamura-Wells J, Li S, Firme MR, Rogic S, Griffith M, Chan S, Yakovenko O, Meyer IM, Zhao EY, Smailus D, Moksa M, Chittaranjan S, Rimsza L, Brooks-Wilson A, Spinelli JJ, Ben-Neriah S, Meissner B, Woolcock B, Boyle M, McDonald H, Tam A, Zhao Y, Delaney A, Zeng T, Tse K, Butterfield Y, Birol I, Holt R, Schein J, Horsman DE, Moore R, Jones SJ, Connors JM, Hirst M, Gascoyne RD and Marra MA. Frequent mutation of histone-modifying genes in non-Hodgkin lymphoma. Nature 2011; 476: 298-303.

[5] Yang F, Zhang L, Huo XS, Yuan JH, Xu D, Yuan SX, Zhu N, Zhou WP, Yang GS, Wang YZ, Shang JL, Gao CF, Zhang FR, Wang F and Sun SH. Long noncoding RNA high expression in hepatocellular carcinoma facilitates tumor growth through enhancer of zeste homolog 2 in humans. Hepatology 2011; 54: 1679-1689.

[6] Gupta RA, Shah N, Wang KC, Kim J, Horlings HM, Wong DJ, Tsai MC, Hung T, Argani P, Rinn JL, Wang Y, Brzoska P, Kong B, Li R, West RB, van de Vijver MJ, Sukumar S and Chang HY. Long non-coding RNA HOTAIR reprograms chromatin state to promote cancer metastasis. Nature 2010; 464: 1071-1076.

[7] Wei G, Luo H, Sun Y, Li J, Tian L, Liu W, Liu L, Luo J, He J and Chen R. Transcriptome profiling of esophageal squamous cell carcinoma reveals a long noncoding RNA acting as a tumor suppressor. Oncotarget 2015; 6: 17065-17080.

[8] Gao HY, Wu B, Yan W, Gong ZM, Sun Q, Wang HH and Yang W. Microarray expression profiles of long non-coding RNAs in germinal center-like diffuse large B-cell lymphoma. Oncol Rep 2017; 38: 1363-1372.

[9] Bo H, Gong Z, Zhang W, Li X, Zeng Y, Liao Q, Chen P, Shi L, Lian Y, Jing Y, Tang K, Li Z, Zhou Y, Zhou M, Xiang B, Li X, Yang J, Xiong W, Li G and Zeng Z. Upregulated long non-coding RNA AFAP1-AS1 expression is associated with progression and poor prognosis of nasopharyngeal carcinoma. Oncotarget 2015; 6: 20404-20418.

[10] Wu W, Bhagat TD, Yang X, Song JH, Cheng Y, Agarwal R, Abraham JM, Ibrahim S, Bartenstein M, Hussain Z, Suzuki M, Yu Y, Chen W, Eng C, Greally J, Verma A and Meltzer SJ. Hypomethylation of noncoding DNA regions and overexpression of the long noncoding RNA, AFAP1-AS1, in Barrett's esophagus and esophageal adenocarcinoma. Gastroenterology 2013; 144: 956-966, e954.

[11] Zhang JY, Weng MZ, Song FB, Xu YG, Liu Q, Wu JY, Qin J, Jin T and Xu JM. Long noncoding RNA AFAP1-AS1 indicates a poor prognosis of hepatocellular carcinoma and promotes cell proliferation and invasion via upregulation of the RhoA/Rac2 signaling. Int J Oncol 2016; 48: 1590-1598.

[12] Hao F, Mou Y, Zhang L, Wang S and Yang Y. LncRNA AFAP1-AS1 is a prognostic biomarker and serves as oncogenic role in retinoblastoma. Biosci Rep 2018; 38: BSR20180384.

[13] Ye Y, Chen J, Zhou Y, Fu Z, Zhou Q, Wang Y, Gao W, Zheng S, Zhao X, Chen T and Chen R. High expression of AFAP1-AS1 is associated with poor survival and short-term recurrence in pancreatic ductal adenocarcinoma. J Transl Med 2015; 13: 137.

[14] Shi D, Wu F, Mu S, Hu B, Zhong B, Gao F, Qing X, Liu J, Zhang Z and Shao Z. LncRNA AFAP1-AS1 promotes tumorigenesis and epithelial-mesenchymal transition of osteosarcoma through RhoC/ROCK1/p38MAPK/Twist1 signaling pathway. J Exp Clin Cancer Res 2019; 38: 375.

[15] Wang ZY, Hu M, Dai MH, Xiong J, Zhang S, Wu HJ, Zhang SS and Gong ZJ. Retraction note: up-

regulation of the long non-coding RNA AFAP1-AS1 affects the proliferation, invasion and survival of tongue squamous cell carcinoma via the Wnt/beta-catenin signaling pathway. Mol Cancer 2019; 18: 104.

[16] Yu S, Yang D, Ye Y, Liu P, Chen Z, Lei T, Pu J, Liu L and Wang Z. Long noncoding RNA actin filament-associated protein 1 antisense RNA 1 promotes malignant phenotype through binding with lysine-specific demethylase 1 and repressing HMG box-containing protein 1 in non-small-cell lung cancer. Cancer Sci 2019; 110: 2211-2225.

[17] Wu XB, Feng X, Chang QM, Zhang CW, Wang ZF, Liu J, Hu ZQ, Liu JZ, Wu WD, Zhang ZP and Liu XQ. Cross-talk among AFAP1-AS1, ACVR1 and microRNA-384 regulates the stemness of pancreatic cancer cells and tumorigenicity in nude mice. J Exp Clin Cancer Res 2019; 38: 107.

[18] Han M, Gu Y, Lu P, Li J, Cao H, Li X, Qian X, Yu C, Yang Y, Yang X, Han N, Dou D, Hu J and Dong H. Exosome-mediated lncRNA AFAP1-AS1 promotes trastuzumab resistance through binding with AUF1 and activating ERBB2 translation. Mol Cancer 2020; 19: 26.

[19] Pfeifer M, Grau M, Lenze D, Wenzel SS, Wolf A, Wollert-Wulf B, Dietze K, Nogai H, Storek B, Madle H, Dorken B, Janz M, Dirnhofer S, Lenz P, Hummel M, Tzankov A and Lenz G. PTEN loss defines a PI3K/AKT pathway-dependent germinal center subtype of diffuse large B-cell lymphoma. Proc Natl Acad Sci U S A 2013; 110: 12420-12425.

[20] Lenz G, Wright GW, Emre NC, Kohlhammer H, Dave SS, Davis RE, Carty S, Lam LT, Shaffer AL, Xiao W, Powell J, Rosenwald A, Ott G, Muller-Hermelink HK, Gascoyne RD, Connors JM, Campo E, Jaffe ES, Delabie J, Smeland EB, Rimsza LM, Fisher RI, Weisenburger DD, Chan WC and Staudt LM. Molecular subtypes of diffuse large B-cell lymphoma arise by distinct genetic pathways. Proc Natl Acad Sci U S A 2008; 105: 13520-13525.

[21] Lohr JG, Stojanov P, Lawrence MS, Auclair D, Chapuy B, Sougnez C, Cruz-Gordillo P, Knoechel B, Asmann YW, Slager SL, Novak AJ, Dogan A, Ansell SM, Link BK, Zou L, Gould J, Saksena G, Stransky N, Rangel-Escareno C, Fernandez-Lopez JC, Hidalgo-Miranda A, Melendez-Zajgla J, Hernandez-Lemus E, Schwarz-Cruz y Celis A, Imaz-Rosshandler I, Ojesina AI, Jung J, Pedamallu CS, Lander ES, Habermann TM, Cerhan JR, Shipp MA, Getz G and Golub TR. Discovery and prioritization of somatic mutations in diffuse large B-cell lymphoma (DLBCL) by whole-exome sequencing. Proc Natl Acad Sci U S A 2012; 109: 3879-3884.

[22] Pasqualucci L, Trifonov V, Fabbri G, Ma J, Rossi D, Chiarenza A, Wells VA, Grunn A, Messina M, Elliot O, Chan J, Bhagat G, Chadburn A, Gaidano G, Mullighan CG, Rabadan R and Dalla-Favera R. Analysis of the coding genome of diffuse large B-cell lymphoma. Nat Genet 2011; 43: 830-837.

[23] Kalkhoven E. CBP and p300: HATs for different occasions. Biochem Pharmacol 2004; 68: 1145-1155.

[24] Pasqualucci L, Dominguez-Sola D, Chiarenza A, Fabbri G, Grunn A, Trifonov V, Kasper LH, Lerach S, Tang H, Ma J, Rossi D, Chadburn A, Murty VV, Mullighan CG, Gaidano G, Rabadan R, Brindle PK and Dalla-Favera R. Inactivating mutations of acetyltransferase genes in B-cell lymphoma. Nature 2011; 471: 189-195.

[25] Zhang X, Zhou Y, Mao F, Lin Y, Shen S and Sun Q. lncRNA AFAP1-AS1 promotes triple negative breast cancer cell proliferation and invasion via targeting miR-145 to regulate MTH1 expression. Sci Rep 2020; 10: 7662.

[26] Liu F, Hu L, Pei Y, Zheng K, Wang W, Li S, Qiu E, Shang G, Zhang J and Zhang X. Long non-coding RNA AFAP1-AS1 accelerates the progression of melanoma by targeting miR-653-5p/RAI14 axis. BMC Cancer 2020; 20: 258.

[27] Yuan Z, Xiu C, Song K, Pei R, Miao S, Mao X, Sun J and Jia S. Long non-coding RNA AFAP1-AS1/miR-320a/RBPJ axis regulates laryngeal carcinoma cell stemness and chemoresistance. J Cell Mol Med 2018; 22: 4253-4262.

[28] Yarosh CA, Iacona JR, Lutz CS and Lynch KW. PSF: nuclear busy-body or nuclear facilitator? Wiley Interdiscip Rev RNA 2015; 6: 351-367.

[29] Gao Z, Chen M, Tian X, Chen L, Chen L, Zheng X, Wang H, Chen J, Zhao A, Yao Q, Zhu Q, Jin S, Hu H, Zeng S and Yu L. A novel human lncRNA SANT1 cis-regulates the expression of SLC47A2 by altering SFPQ/E2F1/HDAC1 binding to the promoter region in renal cell carcinoma. RNA Biol 2019; 16: 940-949.

[30] Ji Q, Zhang L, Liu X, Zhou L, Wang W, Han Z, Sui H, Tang Y, Wang Y, Liu N, Ren J, Hou F and Li Q. Long non-coding RNA MALAT1 promotes tumour growth and metastasis in colorectal cancer through binding to SFPQ and releasing oncogene PTBP2 from SFPQ/PTBP2 complex. Br J Cancer 2014; 111: 736-748.

[31] Wang S, Zhang Q, Wang Q, Shen Q, Chen X, Li Z, Zhou Y, Hou J, Xu B, Li N and Cao X. NEAT1 paraspeckle promotes human hepatocellular carcinoma progression by strengthening IL-6/STAT3 signaling. Oncoimmunology 2018; 7: e1503913.

[32] Karni R, de Stanchina E, Lowe SW, Sinha R, Mu D and Krainer AR. The gene encoding the splicing factor SF2/ASF is a proto-oncogene. Nat Struct Mol Biol 2007; 14: 185-193.

[33] Anczukow O, Rosenberg AZ, Akerman M, Das S, Zhan L, Karni R, Muthuswamy SK and Krainer AR. The splicing factor SRSF1 regulates apoptosis and proliferation to promote mammary epithelial cell transformation. Nat Struct Mol Biol 2012; 19: 220-228.

[34] Cohen-Eliav M, Golan-Gerstl R, Siegfried Z, Andersen CL, Thorsen K, Orntoft TF, Mu D and Karni R. The splicing factor SRSF6 is amplified and is an oncoprotein in lung and colon cancers. J Pathol 2013; 229: 630-639.

[35] Yu B, Qu L, Wu T, Yan B, Kan X, Zhao X, Yang L, Li Y, Liu M, Tian L, Sun Y and Li Q. A novel LncRNA, AC091729.7 promotes sinonasal squamous cell carcinomas proliferation and invasion through binding SRSF2. Front Oncol 2019; 9: 1575.

[36] Kong J, Sun W, Li C, Wan L, Wang S, Wu Y, Xu E, Zhang H and Lai M. Long non-coding RNA LINC01133 inhibits epithelial-mesenchymal transition and metastasis in colorectal cancer by interacting with SRSF6. Cancer Lett 2016; 380: 476-484.

[37] Gherzi R, Chen CY, Ramos A and Briata P. KSRP controls pleiotropic cellular functions. Semin Cell Dev Biol 2014; 34: 2-8.

[38] Gherzi R, Lee KY, Briata P, Wegmuller D, Moroni C, Karin M and Chen CY. A KH domain RNA binding protein, KSRP, promotes ARE-directed mRNA turnover by recruiting the degradation machinery. Mol Cell 2004; 14: 571-583.

[39] Gou Q, Gao L, Nie X, Pu W, Zhu J, Wang Y, Liu X, Tan S, Zhou JK, Gong Y, He J, Wu K, Xie Y, Zhao W, Dai L, Liu L, Xiang R, Wei YQ, Zhang L and Peng Y. Long noncoding RNA AB074169 inhibits cell proliferation via modulation of KHSRP-mediated CDKN1a expression in papillary thyroid carcinoma. Cancer Res 2018; 78: 4163-4174.

Supplementary Materials

ChIRP-MS method

The protocol of ChIRP was as shown below: (1) Re-suspend cells with pre-cooling PBS buffer, cross link with 3% formaldehyde at room temperature on an end-to-end shaker for 30 min. Quench crosslinking with 125 mM glycine for 5 min, spin at 1000 RCF for 3 min and discard supernatant, wash cell pellets twice with cooling PBS. (2) For each 2×~10^7 cells, add 1 mL Lysis Buffer, sonicate cell lysate in an ice-water bath and check every 10 min until the cell lysate is no longer turbid. Spin at top speed, transfer supernatant to 2 volume of Hybridization Buffer, mix well and incubate at 37°C. (3) Pre-bind probe (4 for TT, 1 for NC and PC, 100 pmol per 2×10^7 cells) to streptavidin beads for 30 min, wash out unbinding probe, and mix with cell lysate, hybridize at 37°C overnight on an end-to-end shaker. (4) Wash beads 5 times with 1 mL pre-warming Wash Buffer, 5 min per washing. At the last washing, transfer 1/20 beads for qPCR analysis. (5) Add 100 μL Elution Buffer, 20 U Benzonase, elute protein at 37°C for 1 h. Transfer supernatant to new low binding eppendorf tube. Wash beads with 100 μL Elution Buffer once, and combine 2 supernatants. (6) Reverse cross-linked sample at 95°C, precipitate protein with 0.1% SDC and 10% TCA at 4°C 2 h. Spin at top speed, wash pellets with pre-cold 80% acetone 3 times.

For each sample, ~1/2 peptide were separated and analyzed with a nano-UPLC (EASY-nLC1200) coupled to Q-Exactive mass spectrometry (Thermo Finnigan). Separation was performed using a reversed-phase column (100 μm, ID×15 cm, Reprosil-Pur 120 C18-AQ, 1.9 μm, Dr. Math). Mobile phases were H2O with 0.1% FA, 2% ACN (phase A) and 80% ACN, 0.1% FA (phase B). Separation of sample was executed with a 120 min gradient at 300 nL/min flow rate. Gradient B: 8 to 30% for 92 min, 30 to 40% for 20 min, 40 to 100% for 2 min, 100% for 2 min, 100 to 2% for 2 min and 2% for 2 min. Data dependent acquisition was performed in profile and positive mode with Orbitrap analyzer at a resolution of 70,000 (@200 m/z) and m/z range of 350-1600 for MS1; For MS2, the resolution was set to 17,500 with a dynamic first mass. The automatic gain control (AGC) target for MS1 was set to 1.0E+6 with max IT 100 ms, and 5.0E+4 for MS2 with max IT 200 ms. The top 10 most intense ions were fragmented by HCD with normalized collision energy (NCE) of 27%, and isolation window of 2 m/z. The dynamic exclusion time window was 20 s.

Raw MS files were processed with MaxQuant (Version 1.5.6.0). The protein sequence database (Uniprot_organism_2016_09) was downloaded from UNIPROT. This database and its reverse decoy were then searched against by MaxQuant software. Trypsin was set as specific enzyme with up to 3 miss cleavage; Oxidation [M] and Acetyl [protein N-term] were considered as variable modification (max number of modifications per peptide is 3), Carbamidomethyl [C] was set as fixed modification; Both peptide and protein FDR should be less than 0.01. Only unique & razor peptides were used for quantification. All the other parameters were reserved as default.

Supplementary Table 1. Sequences of shRNAs

sh-AFAP1-AS1#1	top strand	AATTCGCGGCTCTACTGAACTGG CATCAAATTTCAAGAGAATTTGATGCCAGTTCAGTAGAGCCGTTTTTTG
	bottom strand	GATCCAAAAAACGGCTCTACTGAACTGGCATCAAATTCTCTT GAAATTTGATGCCAGTTCAGTAGAGCCGCG
sh-AFAP1-AS1#2	top strand	AA TTCGAACACCAATCCCAAGAGGTGATTCAAGAGATCACCTCTTGGGATTGGTGTTTTTTTTG
	bottom strand	GATCCAAAAAAAACACCAATCCCAAGAG GTGATCTCTTGAATCACCTCTTGGGATTGGTGTTCG
sh-AFAP1-AS1#3	top strand	AATTCGCCATGTCATCTGACTGGCTCTGAATTCAAGAGATTCAGAGC CAGTCAGATGACATGGCTTTTTTG
	bottom strand	GATCCAAAAAAGCCA TGTCATCTGACTGGCTCTGAATCTCTTGAATTCAGAGCCAGTCAGATGACATGGCG
sh-NC	top strand	AATTCGTTCTCCGAACGTGTCACGTAATTCAAGAG ATTACGTGACACGTTCGGAGAATTTTTTG
	bottom strand	GATCCAAAAA ATTCTCCGAACGTGTCACGTAATCTCTTGAATTACGTGACACGTTCGGAGAACG

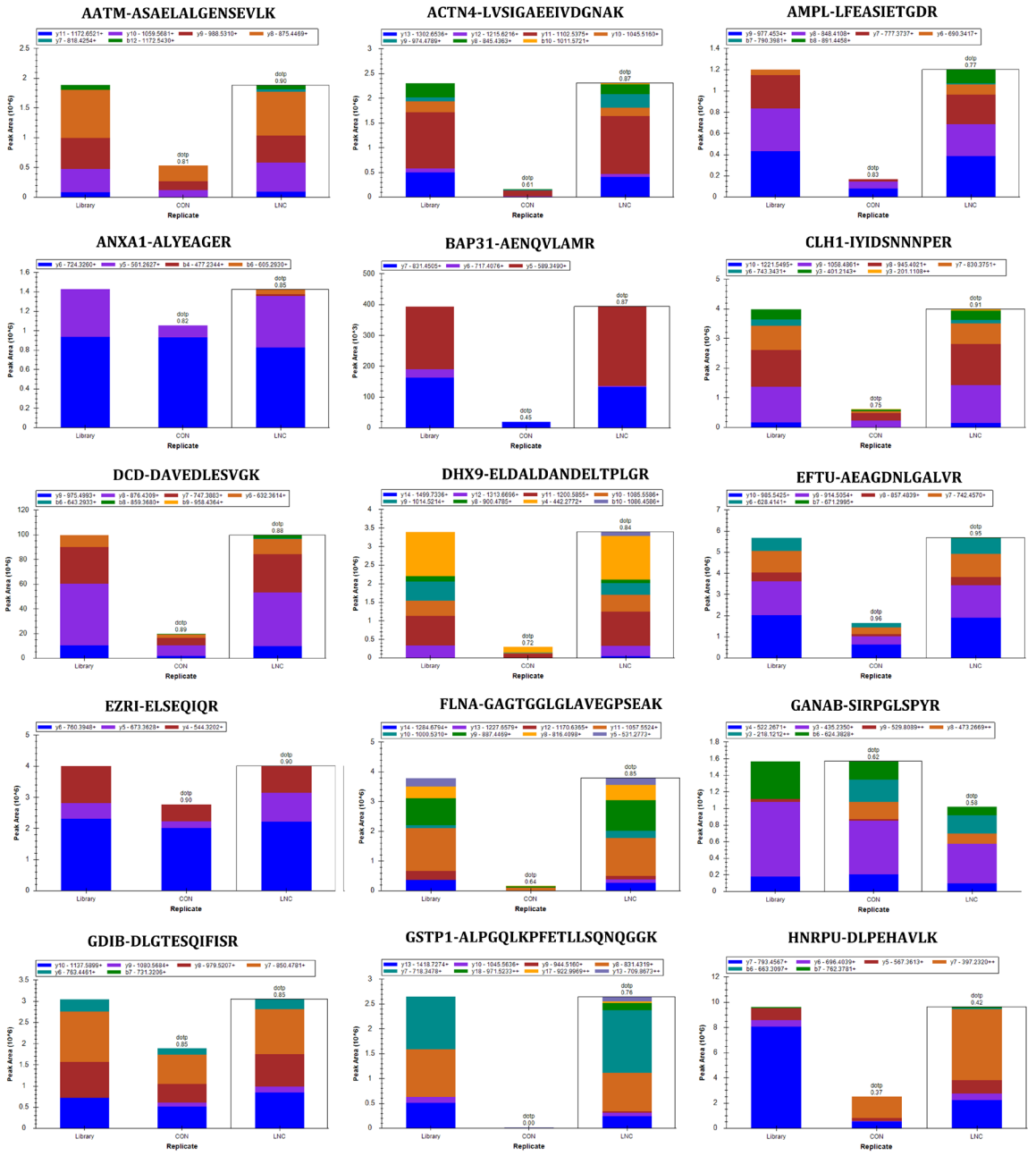

Supplementary Figure 1. Validation of ChIRP-MS results by PRM. Histograms for the quantitative comparison of the peptides of specific proteins (AATM, ACTN4, AMPL, ANXA1, BAP31, CLH1, DCD, DHX9, EFTU, EZRI, FLNA, GANAB, GDIB, GSTP1, and HNRPU) between the sample groups.

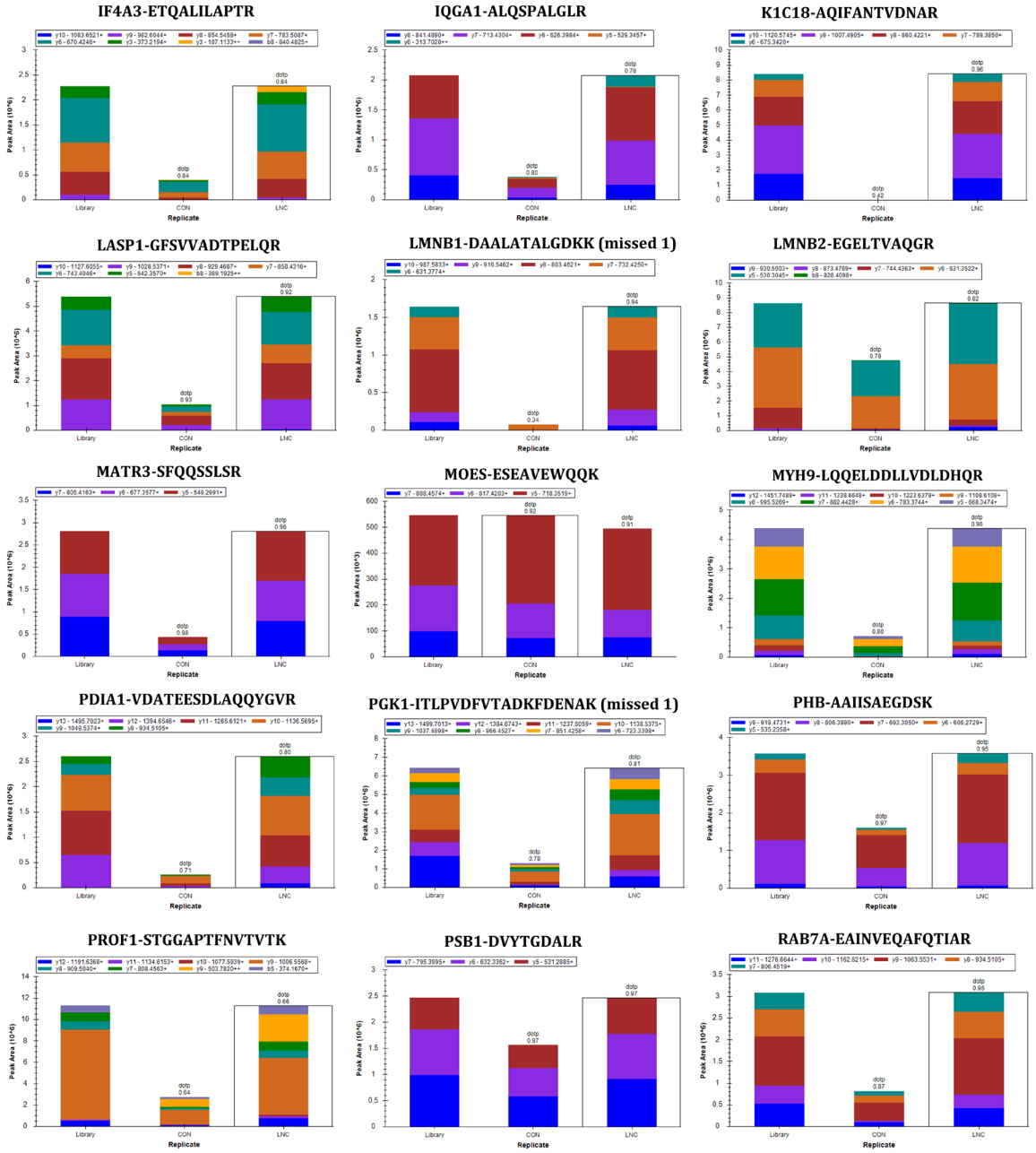

Supplementary Figure 2. Validation of ChIRP-MS results by PRM. Histograms for the quantitative comparison of the peptides of specific proteins (IF4A3, IQGA1, K1C18, LASP1, LMNB1, LMNB2, MATR3, MOES, MYH9, PDIA1, PGK1, PHB, PROF1, PSB1, and RAB7A) between the sample groups.

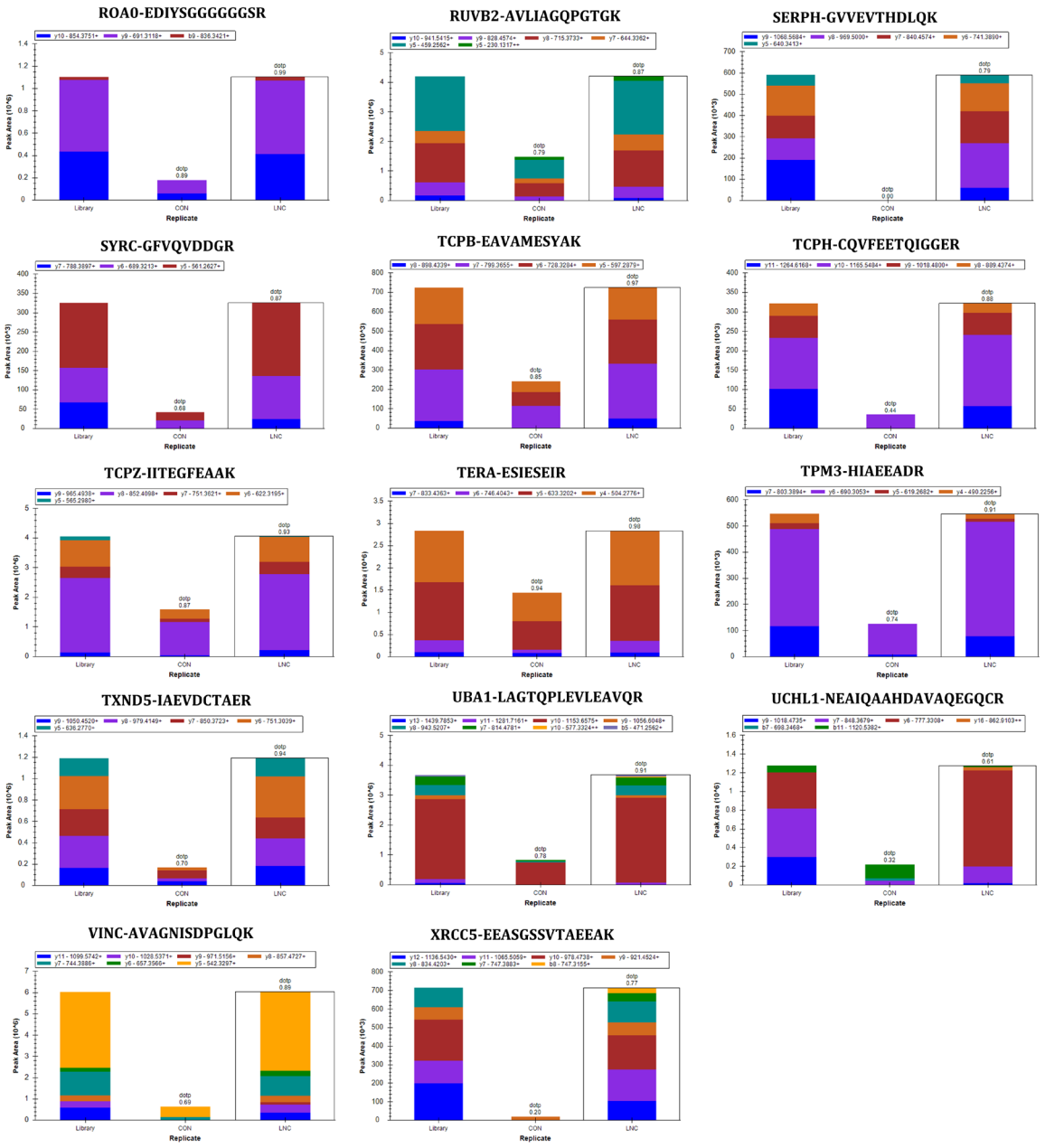

Supplementary Figure 3. Validation of ChIRP-MS results by PRM. Histograms for the quantitative comparison of the peptides of specific proteins (ROA0, RUVB2, SERPH, SYRC, TCPB, TCPH, TCPZ, TERA, TPM3, TXND5, UBA1, UCHL1, VINC, XRCC5) between the sample groups.